

Mitochondrial function-associated genes underlie cortical atrophy in prodromal synucleinopathies

Shady Rahayel,^{1,2} Christina Tremblay,¹ Andrew Vo,¹ Bratislav Mistic,¹ Stéphane Lehericy,³ Isabelle Arnulf,³ Marie Vidailhet,³ Jean-Christophe Corvol,³ the ICEBERG Study Group,³ Jean-François Gagnon,^{2,4,5} Ronald B. Postuma,^{2,6} Jacques Montplaisir,^{2,7} Simon Lewis,⁸ Elie Matar,⁸ Kaylena Ehgoetz Martens,^{8,9} Per Borghammer,¹⁰ Karoline Knudsen,¹⁰ Allan K. Hansen,¹⁰ Oury Monchi,^{5,11,12} Ziv Gan-Or^{1,12,13,†} and Alain Dagher^{1,12,†} for the Alzheimer's Disease Neuroimaging Initiative

[†]These authors contributed equally to this work.

Abstract

Isolated rapid eye movement sleep behaviour disorder (iRBD) is a sleep disorder characterized by the loss of rapid eye movement sleep muscle atonia and the appearance of abnormal movements and vocalizations during rapid eye movement sleep. It is a strong marker of incipient synucleinopathy such as dementia with Lewy bodies and Parkinson's disease. Patients with iRBD already show brain changes that are reminiscent of manifest synucleinopathies including brain atrophy. However, the mechanisms underlying the development of this atrophy remain poorly understood.

In this study, we performed cutting-edge imaging transcriptomics and comprehensive spatial mapping analyses in a multicentric cohort of 171 polysomnography-confirmed iRBD patients (67.7 ± 6.6 (49-87) years; 83% men) and 238 healthy controls (66.6 ± 7.9 (41-88) years; 77% men) with T1-weighted MRI to investigate the gene expression and connectivity patterns associated with changes in cortical thickness and surface area in iRBD. Partial least squares regression was performed to identify the gene expression patterns underlying cortical changes in iRBD. Gene set enrichment analysis and virtual histology were then done to assess the biological processes, cellular components, human disease gene terms, and cell types enriched in these gene expression patterns. We then used structural and functional neighbourhood analyses to assess whether the atrophy patterns in iRBD were constrained by the brain's structural and functional connectome. Moreover,

1 we used comprehensive spatial mapping analyses to assess the specific neurotransmitter systems,
2 functional networks, cytoarchitectonic classes, and cognitive brain systems associated with cortical
3 changes in iRBD. All comparisons were tested against null models that preserved spatial
4 autocorrelation between brain regions and compared to Alzheimer's disease to assess the
5 specificity of findings to synucleinopathies.

6 We found that genes involved in mitochondrial function and macroautophagy were the strongest
7 contributors to the cortical thinning occurring in iRBD. Moreover, we demonstrated that cortical
8 thinning was constrained by the brain's structural and functional connectome and that it mapped
9 onto specific networks involved in motor and planning functions. In contrast with cortical
10 thickness, changes in cortical surface area were related to distinct genes, namely genes involved in
11 the inflammatory response, and to different spatial mapping patterns. The gene expression and
12 connectivity patterns associated with iRBD were all distinct from those observed in Alzheimer's
13 disease.

14 In summary, this study demonstrates that the development of brain atrophy in synucleinopathies is
15 constrained by specific genes and networks.

16
17 **Author affiliations:**

18 1 The Neuro (Montreal Neurological Institute-Hospital), McGill University, Montreal H3A 2B4,
19 Canada

20 2 Centre for Advanced Research in Sleep Medicine, Hôpital du Sacré-Cœur de Montréal, Montreal
21 H4J 1C5, Canada

22 3 Sorbonne Université, Institut du Cerveau – Paris Brain Institute – ICM, INSERM, CNRS, Paris
23 75013, France

24 4 Department of Psychology, University of Quebec in Montreal, Montreal H2X 3P2, Canada

25 5 Research Centre, Institut universitaire de gériatrie de Montréal, Montreal H3W 1W5, Canada

26 6 Department of Neurology, Montreal General Hospital, Montreal H3G 1A4, Canada

27 7 Department of Psychiatry, University of Montreal, Montreal H3T 1J4, Canada

1 8 ForeFront Parkinson's Disease Research Clinic, Brain and Mind Centre, University of Sydney,
2 Camperdown NSW 2050, Australia

3 9 Department of Kinesiology, University of Waterloo, Waterloo N2L 3G1, Canada

4 10 Department of Nuclear Medicine and PET, Aarhus University Hospital, Aarhus DK-8200,
5 Denmark

6 11 Department of Radiology, Radio-Oncology, and Nuclear Medicine, University of Montreal,
7 Montreal H3T 1A4, Canada

8 12 Department of Neurology and Neurosurgery, McGill University, Montreal H3A 1A1, Canada

9 13 Department of Human Genetics, McGill University, Montreal H3A 0C7, Canada

10

11 Correspondence to: Shady Rahayel, PsyD, PhD

12 The Neuro (Montreal Neurological Institute-Hospital), McGill University

13 3801 University Street

14 Montreal, Quebec, Canada

15 H3A 2B4

16 E-mail: shady.rahayel@mcgill.ca

17 **Running title:** Mitochondria underlie thinning in iRBD

18

19 **Keywords:** REM sleep behaviour disorder; Parkinson's disease; dementia with Lewy bodies;
20 transcriptomics; network analysis; MRI

21

22 **Introduction**

23 Isolated rapid eye movement sleep behaviour disorder (iRBD) is a parasomnia characterized by
24 abnormal movements and vocalizations during rapid eye movement sleep that typically develops
25 into dementia with Lewy bodies, Parkinson's disease, and multiple system atrophy.^{1,2} As a
26 prodromal synucleinopathy, iRBD patients show brain changes like those seen in manifest

1 synucleinopathies.³ In particular, brain atrophy has been shown to occur in iRBD patients,⁴
2 correlates with clinical changes,⁵⁻⁸ especially cognitive impairment,⁶ and predicts the
3 phenoconversion to dementia with Lewy bodies compared to Parkinson's disease.⁹ However, to
4 date, the mechanisms underlying the development of brain atrophy and its patterns in iRBD remain
5 poorly understood.

6 A collection of observations in humans and experimental findings in animals support the notion
7 that the pathology arises from a prion-like spreading occurring within a brain environment
8 characterized by some cells being more selectively vulnerable to pathology than others.¹⁰⁻¹² A
9 recent study tested the prion-like spreading hypothesis and the selective vulnerability hypothesis
10 using an agent-based computational model that simulates (in silico) the propagation of alpha-
11 synuclein based on local gene expression and connectivity.¹³ The simulations derived from this
12 model were shown to recreate the distribution of alpha-synuclein pathology in the mouse brain
13 after the injection of preformed fibrils.¹⁴ When applied to iRBD and Parkinson's disease, this model
14 demonstrated that the patterns of atrophy could be recreated computationally and that both gene
15 expression and connectivity were determinant factors shaping atrophy.^{13,15,16} However, in these
16 studies, only the regional expression of two genes, *SNCA* and *GBA*, was used to model the agents'
17 spread, thus limiting the breadth of understanding of the wider genetic correlates that may underlie
18 structural brain changes in synucleinopathies. To our knowledge, no study has yet investigated the
19 patterns of gene expression associated with cortical changes in iRBD.

20 Imaging transcriptomics is a recent approach that allows a multivariate investigation into the
21 associations between brain anatomy and the transcriptional activity of genes across the whole
22 brain.¹⁷ In Parkinson's disease, this approach has revealed that the regions showing greater
23 progression of atrophy over two and four years had a greater expression of genes involved in
24 synaptic activity and cell signalling.¹⁸ Furthermore, the computational modelling of atrophy spread
25 in Parkinson's disease has also revealed the involvement of transcripts associated with immune
26 and lysosomal functions.^{19,20} Imaging transcriptomics has also demonstrated that increased brain
27 iron content in Parkinson's disease related to genes implicated in metal detoxification and synaptic
28 transmission/signalling.²¹ In addition, by virtue of arising from a pathological process that spreads
29 through the connectome, many studies have shown that atrophy in neurodegenerative diseases is
30 shaped by connectivity.^{13,15,22,23} In Parkinson's disease, the progression of atrophy was shown to
31 map onto specific major functional networks, being significantly more pronounced in the limbic,

1 default mode, and visual networks after 2 years, and then extending to almost all networks in the
2 following years.¹⁸ To our knowledge, the gene expression and connectomics underpinnings of
3 cortical changes in prodromal synucleinopathies remain to be investigated.

4 Since iRBD is an early stage during which clinical features of synucleinopathies are still modest,
5 identifying abnormalities on MRI scans and understanding their underlying mechanisms may offer
6 new insights into potential therapies aimed at slowing or stopping the neurodegenerative process
7 in patients. In this study, our objective was to combine imaging transcriptomics and comprehensive
8 spatial mapping to investigate the normal gene expression and connectivity characteristics of the
9 cortical regions most affected in iRBD. Using a large cohort of polysomnography-confirmed iRBD
10 patients and controls with T1-weighted MRI imaging, we used partial least squares (PLS)
11 regression to identify the gene expression patterns associated with cortical thinning in iRBD and
12 investigated the biological processes, cellular components, human disease gene terms, and cell type
13 enrichment in these patterns. We next investigated if the patterns of cortical thinning in iRBD
14 mapped onto specific neurotransmitter systems, functional networks, cytoarchitectonic classes, and
15 spatial patterns related to cognitive functions. Next, we assessed whether these patterns were
16 specific to cortical thinning by assessing the gene expression and spatial mapping patterns
17 underlying the changes in cortical surface area in iRBD. Finally, to understand whether the patterns
18 were specific to synucleinopathies, the imaging transcriptomics and spatial mapping analyses were
19 repeated in patients with Alzheimer's disease. We hypothesized that specific gene expression and
20 spatial mapping patterns would underlie cortical thinning in iRBD and that these patterns would be
21 specific to cortical thickness compared to surface area and to iRBD compared to Alzheimer's
22 disease.

24 **Materials and methods**

25 **Participants**

26 A total of 443 participants (182 polysomnography-confirmed iRBD patients and 261 age- and sex-
27 matched controls) with T1-weighted MRI were recruited from the Movement Disorders clinic at
28 the Hôpital de la Pitié-Salpêtrière (France), the Centre for Advanced Research on Sleep Medicine
29 at the Hôpital du Sacré-Cœur de Montréal (Canada), the ForeFront Parkinson's Disease Research

1 Clinic at the University of Sydney (Australia), Aarhus University Hospital (Denmark), and the
2 Parkinson's Progression Markers Initiative baseline cohort.²⁴ The participants were part of a
3 previous study that assessed brain atrophy in iRBD (Table 1 for demographics and clinical
4 variables of the different cohorts).¹⁵ For up-to-date information on the Parkinson's Progression
5 Markers Initiative database, visit www.ppmi-info.org. All patients received a polysomnography-
6 proven diagnosis based on the International Classification of Sleep Disorders, third edition.²⁵ The
7 absence of concomitant dementia with Lewy bodies, Parkinson's disease or multiple system
8 atrophy was confirmed at the neurological evaluation closest in time to the MRI acquisition.²⁶⁻²⁸
9 All participants were part of research protocols approved by local ethics committees, and the
10 project was approved by the Research Ethics Board of the McGill University Health Centre.

11 **MRI acquisition**

12 MRI acquisition was performed in every centre to acquire T1-weighted images. The Montreal
13 cohort underwent T1-weighted imaging with a 3T Siemens TIM Trio scanner with a 12-channel
14 head coil, MPRAGE sequence with the following parameters: TR: 2300 ms, TE: 2.91 ms, flip
15 angle: 9°, and voxel size: 1 mm³ isotropic. The Paris cohort underwent T1-weighted imaging with
16 a 3T Siemens TIM Trio scanner with a 12-channel head coil, MPRAGE sequence: TR: 2300 ms,
17 TE: 4.18 ms, TI: 900 ms, flip angle: 9°, and voxel size: 1 mm³ isotropic; or a 3T PRISMA Fit
18 scanner with a 64-channel head coil, MP2RAGE sequence: TR: 5,000 ms, TE: 2.98 ms, TI: 700
19 and 2500 ms, flip angle: 4° and 5°, GRAPPA: 3, and voxel size: 1 mm³ isotropic. The Sydney
20 cohort was imaged with a GE Discovery MR750 3T scanner with an 8-channel head coil, BRAVO
21 sequence: TR: 5800 ms, TE: 2.6 ms, flip angle: 12°, and voxel size: 1 mm³ isotropic. The Aarhus
22 cohort was imaged with a 3T Siemens MAGNETOM Skyra scanner with a 32-channel head coil,
23 MPRAGE sequence: TR: 2,420 ms, TE: 3.7 ms, TI: 960 ms, flip angle: 9°, and voxel size: 1 mm³
24 isotropic. The T1-weighted images from the Parkinson's Progression Markers Initiative cohort are
25 described elsewhere.²⁴

26 **Quantification of atrophy**

27 Quantification of cortical thickness and surface area was performed previously.¹⁵ Briefly, from the
28 443 scans available, 409 passed quality control and underwent surface-based processing with
29 FreeSurfer (version 6.0.0) to generate cortical thickness and surface area maps. All maps were

1 inspected visually by a trained rater (S.R.)^{29,30} and excluded if major reconstruction errors (score
2 >2) were found, yielding 345 maps from 138 iRBD patients and 207 controls matched for age
3 (iRBD: 67.0 ± 6.3 years, controls: 66.2 ± 7.6 , $P = 0.28$) and sex (iRBD: 81% men, controls: 77%
4 men, $P = 0.34$). Cortical thickness and surface area values were parcellated using the 34-region
5 Desikan-Killiany atlas and W -scored to control the effects of age, sex, and centre observed in
6 controls.^{31,32} For the purpose of W -scoring, the Parkinson's Progression Markers Initiative data
7 were treated as coming from one single centre. Since cortical surface area scales with head size,³³
8 surface area values were divided by the total intracranial volume before W -scoring. Cortical
9 thickness and surface area W -scores were then z -scored and entered in separate PLS regression
10 models to investigate their associations with whole-brain transcriptional activity. The primary
11 analyses were done with cortical thickness as the predicted variable to understand the bases of
12 cortical atrophy in iRBD; the same analyses were repeated with surface area to investigate the
13 contrast between different cortical metrics.

14 **Regional gene expression extraction**

15 To assess the genetic features of the regions showing cortical changes in iRBD, we extracted from
16 the Allen Human Brain Atlas the regional gene expression data from the same 34 regions used for
17 measuring atrophy.³⁴ The Allen Human Brain Atlas provides the expression of more than 20,000
18 genes quantified across 3,702 brain tissue samples from 6 post-mortem brains.³⁵ Its whole-brain
19 spatial coverage makes it the most comprehensive gene expression atlas of the adult human brain
20 to date, and it is widely used in imaging transcriptomics for extracting regional gene expression
21 data from user-defined parcellations.¹⁷

22 For the main analyses, we extracted the microarray data from the 6 post-mortem brains (ages: 24,
23 31, 39, 49, 55, and 57 years old; 5 (83%) male and 1 (17%) female) provided by the Allen Human
24 Brain Atlas using *abagen* (version 0.1.3; <https://github.com/rmarkello/abagen>).³⁵ First, microarray
25 probes were reannotated based on previous data;³⁶ probes not matched to a valid Entrez ID were
26 discarded. Probes were then filtered based on their expression intensity relative to background
27 noise,³⁷ such that probes with intensity less than the background in $\geq 50\%$ of samples across donors
28 were discarded. When multiple probes indexed the expression of the same gene, we selected and
29 used the probe with the most consistent pattern of regional variation across donors (i.e., differential
30 stability):³⁸

1

$$\Delta_s(p) = \frac{1}{\binom{N}{2}} \sum_{i=1}^{N-1} \sum_{j=i+1}^N \rho[B_i(p), B_j(p)] \quad (1)$$

2

3

4

5

where ρ is Spearman's rank correlation of the expression of a single probe p across regions in two donors B_i and B_j , and N is the total number of donors. Here, regions corresponded to the structural designations provided in the ontology from the Allen Human Brain Atlas.³⁴

6

7

8

9

10

11

12

13

The Montreal Neurological Institute coordinates of tissue samples were updated to those generated via non-linear registration using Advanced Normalization Tools (<https://github.com/chrisfilo/alleninf>). Samples were assigned to brain regions in the provided atlas if their Montreal Neurological Institute coordinates were within 2 mm of a given parcel. To reduce the potential for misassignment, sample-to-region matching was constrained by hemisphere and gross structural divisions (i.e., cortex, subcortex/brainstem, and cerebellum, such that e.g., a sample in the left cortex could only be assigned to an atlas parcel in the left cortex).³⁶ All tissue samples not assigned to a brain region in the provided atlas were discarded.

14

15

16

Inter-subject variation was addressed by normalizing tissue sample expression values across genes using a robust sigmoid function:³⁹

$$x_{norm} = \frac{1}{1 + \exp\left(-\frac{(x - \langle x \rangle)}{IQR_x}\right)} \quad (2)$$

17

18

19

20

where $\langle x \rangle$ is the median and IQR_x is the normalized interquartile range of the expression of a single tissue sample across genes. Normalized expression values were then rescaled to the unit interval:

$$x_{scaled} = \frac{x_{norm} - \min(x_{norm})}{\max(x_{norm}) - \min(x_{norm})} \quad (3)$$

21

1 Gene expression values were then normalized across tissue samples using an identical procedure.
2 Samples assigned to the same brain region were averaged separately for each donor and then across
3 donors, yielding a regional expression matrix. Since 4 of the 6 post-mortem brains did not have
4 available gene expression in the right hemisphere, the main analyses were performed using the
5 gene expression from the left hemisphere. The resulting gene expression region of interest values
6 were z -scored, entered as predictors in PLS regression, and used for the main analyses performed
7 in this study.

8 Although the gene expression data were extracted from post-mortem brains with similar sex
9 proportion (83% male, 17% female) as in the iRBD (81% male, 19% female) and control groups
10 (77% male, 23% female), the average age differed significantly (post-mortem brains: 42.5 ± 13.4
11 years, $P = 0.006$ versus iRBD, $P = 0.007$ versus controls). We therefore tested whether our findings
12 were robust to age effects on gene expression by extracting different subsets of gene expression
13 from the post-mortem brains, namely from the two oldest brains (55 and 57 years, average: 56.0
14 years), from the three older post-mortem brains (49, 55, and 57 years old, average: 53.7 years), and
15 using a leave-one-out procedure whereby one of the six brains was left out at each iteration and
16 gene expression calculated on the remaining five brains (average age at each iteration: 39.6, 40.0,
17 41.2, 43.2, 44.8, and 46.2 years old). In addition, to investigate the effect of laterality, we also
18 extracted the gene expression data from the right hemisphere (2 of the 6 brains) and repeated these
19 analyses with these data.

20 **PLS regression**

21 PLS regression was used to identify the pattern of gene expression associated with cortical
22 thickness W -scores in iRBD. PLS regression performs a dual decomposition of two matrices \mathbf{X} and
23 \mathbf{Y} to derive components from \mathbf{X} (34 regions x 15,633 genes) that account for the maximal amount
24 of covariance explained by \mathbf{Y} (34 thickness W -scores). To test significance, the empirical variance
25 explained by each component was tested against the variance observed in 10,000 null models in
26 which atrophy was randomly permuted between regions (random null models). Since the brain is
27 characterized by a high level of spatial autocorrelation between regions,⁴⁰ to demonstrate that the
28 gene-atrophy associations were not due to lower-order spatial gradients, the empirical variance was
29 compared to 10,000 spatially-constrained null models in which regions were shuffled using a
30 spherical reassignment procedure that preserved spatial autocorrelation between regions (spatial

1 null models).⁴⁰ A PLS component was considered significant when fewer than 5% of the null
2 models explained more variance than the original atrophy vector.

3 To identify the genes that contributed the most to the components associated with cortical changes,
4 a bootstrapping resampling procedure was performed by randomly shuffling the rows of **X** and **Y**
5 and by repeating the PLS regression with the shuffled matrices; this was repeated 5,000 times to
6 generate the null distribution and standard errors for each gene expression weight. Bootstrap ratios
7 were calculated as the ratio between the weight of each gene expression and its bootstrap-estimated
8 standard error and interpreted as a *z*-score.⁴¹ The gene lists were then ranked from the highest to
9 the lowest scores based on the bootstrap ratios and used as inputs for gene set enrichment analysis
10 (GSEA).

11 **Gene enrichment analyses**

12 To examine the translational relevance of transcriptomic correlates of atrophy in iRBD,
13 WebGestalt 2019 (<http://www.webgestalt.org>)⁴² was used to perform GSEA and identify the
14 biological processes, cellular components, and human diseases gene terms enriched in the genes
15 predicting cortical thickness *W*-scores in iRBD. GSEA assesses whether the genes located at the
16 top or bottom of a ranked gene list, in this case derived from the bootstrapping resampling
17 procedure, occurred more frequently than expected by chance.⁴³ The Gene Ontology knowledge
18 base (April 2019, <http://geneontology.org>) was used for biological process and cellular component
19 gene terms, whereas the DisGeNET (version 5.0, May 2017, <https://www.disgenet.org>), Online
20 Mendelian Inheritance in Man (OMIM; <https://www.omim.org>), and GLAD4U (November 2018,
21 <http://glad4u.zhang-lab.org/index.php>) knowledge bases were used separately for human disease
22 gene terms. The minimal and maximal number of genes for enrichment was set to 3 and 2,000,
23 respectively. Statistical correction for multiple testing was performed by running 1,000 random
24 permutations and adjusting *P*-values with the false discovery rate (FDR) method; for
25 interpretability, only the top ten most significant terms retrieved on the positive and negative ends
26 were interpreted.

27 We also performed over-representation analysis in WebGestalt 2019 to investigate whether the
28 genes most reliably associated with thickness *W*-scores were enriched for gene terms related to
29 specific biological processes, cellular components, and human diseases compared to the complete
30 gene set. The target list was composed of the genes with a bootstrap ratio weight ± 5.0

1 (corresponding to z -scores less than $P < 0.0001$), whereas the background list was composed of all
2 the genes extracted from the Allen Human Brain Atlas. To ensure that the enrichment patterns were
3 not due to the choice of a particular gene ontology platform, we repeated the over-representation
4 analyses using GOrilla (<http://cbl-gorilla.cs.technion.ac.il>)⁴⁴ to assess the biological process and
5 cellular component gene terms enriched in the target lists (i.e., negatively or positively weighted
6 genes with bootstrap ratios ± 5.0) compared to the same background list. We also repeated the PLS
7 regression and gene enrichment analyses using the gene expression matrices extracted from the
8 different subsets of post-mortem brains (i.e., oldest brains, older brains, and using the leave-one-
9 out procedure) and from the post-mortem brains with right hemisphere gene expression data.

10 **Virtual histology**

11 We next used virtual histology to investigate whether the genes predicting cortical thickness W -
12 scores in iRBD were enriched for specific brain cell types. Using single-cell RNA sequencing from
13 five post-mortem studies performed on human cortical samples (see Seidlitz et al. for a description
14 of the different samples),^{18,45} the regional expression of the genes associated with astrocytes,
15 endothelial cells, microglia, excitatory neurons, inhibitory neurons, oligodendrocytes, and
16 oligodendrocyte precursor cells were extracted for the 34 regions and averaged across genes to
17 generate an average regional gene expression for each of the 7 cell types.⁴⁶ Spearman's correlation
18 coefficients were computed between each cell type's average regional gene expression and the
19 regional cortical thickness W -scores. An association was considered significant when below the
20 Bonferroni-corrected threshold of $P < 0.0071$ (7 correlations) and tested against 10,000 null models
21 with and without preservation of the spatial autocorrelation between brain regions.

22 **Structural and functional neighbourhood analysis**

23 According to the prion-like spread hypothesis, pathology propagates between cells by following
24 the constraints imposed by the brain's architecture (connectivity).⁴⁷ Here, we tested whether
25 structural and functional connectivity constrained the cortical changes observed in iRBD by
26 assessing whether the cortical thickness W -scores of each region were associated with the average
27 cortical thickness W -scores measured in the structurally or functionally connected neighbours of
28 each region. Unlike analyses involving gene expression, which were restricted to the left
29 hemisphere, these network analyses were performed using both hemispheres. To identify the

1 structural and functional neighbours of each region, the diffusion-weighted and resting-state
 2 functional MRI data from 70 healthy participants (28.8 ± 9.1 years, 27 females) were used to
 3 generate individual structural and functional connectivity maps. These data were processed
 4 previously⁴⁸ and used in several studies assessing the impact of connectivity on atrophy.^{18,49-51}
 5 After exclusion of 4 connectivity maps with aberrant scores (3 structural, 1 functional), the
 6 individual structural matrices were transformed into a group-consensus structural connectivity
 7 matrix that preserved the brain's edge length distribution;⁵² self-connections were converted to
 8 zero.

9 To assess the impact of structural connectivity, the structural neighbourhood change D_i was
 10 quantified by averaging the structural change observed in the total number N of nodes j that had a
 11 structural connection with each region i (i.e., structural neighbours):

$$D_i = \frac{1}{N_i} \sum_{j \neq i, j=1}^{N_i} |d_j| \quad (4)$$

13
 14 To assess the impact of functional connectivity, the functional neighborhood change was calculated
 15 by averaging the structural change observed in all the structural neighbours j weighted by the
 16 strength of the functional connection between region i and neighbour j (FC_{ij}):

$$D_i = \frac{1}{N_i} \sum_{j \neq i, j=1}^{N_i} |d_j| * FC_{ij} \quad (5)$$

17
 18
 19 Spearman's correlation coefficients were calculated between the cortical thickness W -scores in
 20 iRBD, and the structural and functional neighbourhood change quantified in each region. The
 21 empirical correlation coefficients were tested against the correlations observed in sets of 10,000
 22 randomized spatial and random null models. Additional analyses were also performed to
 23 investigate the correlations between the local cortical thickness W -scores in every region and the

1 average change observed in regions that were not part of the region's structural or functional
2 neighbourhood.

3 **Spatial mapping of cortical changes to brain systems**

4 We performed a comprehensive mapping study of the cortical changes in iRBD by assessing
5 whether the thickness *W*-scores were significantly more pronounced in specific brain systems,
6 namely neurotransmitter systems, intrinsic functional networks, cytoarchitectonic classes, and
7 spatial correlates of cognitive functions. For the neurotransmitter systems, the previously curated
8 regional density maps of 18 receptors, transporters, and receptor binding sites associated with
9 dopamine (D1,⁵³ D2,^{54,55} dopamine transporter (DAT)⁵⁶), serotonin (5-HT_{1A},⁵⁷ 5-HT_{1B},^{57,58} 5-
10 HT_{2A},⁵⁹ 5-HT₄,⁵⁹ 5-HT₆,⁶⁰ serotonin transporter (5-HTT)⁵⁹), noradrenaline (noradrenaline
11 transporter (NET)),⁶¹ acetylcholine (α 4 β 2,⁶² M₁,⁶³ vesicular acetylcholine transporter
12 (VACHT)^{46,64,65}), GABA (GABA_{A/BZ}),⁶⁶ glutamate (mGluR5),^{46,67,68} histamine (H₃),⁶⁹
13 endocannabinoids (CB₁),⁷⁰ and opioids (μ),⁷¹ were generated from the PET images of 1,238 healthy
14 individuals (718 males and 520 females between 18 and 68 years old depending on the tracer; see
15 Supplementary Table 3 in Hansen et al. for demographic and methodological details for each PET
16 tracer).⁴⁶ These maps were parcellated into the same 68 regions used for measuring atrophy and
17 separately *z*-scored. When several maps were available for a tracer, a weighted average map was
18 generated based on the number of subjects used for each map. Spearman's correlation coefficients
19 were used to test the association between cortical thickness *W*-scores and the regional density of
20 each map. Correlations surviving the Bonferroni-corrected threshold for each set of associations
21 ($P < 0.0028$) were tested against sets of 10,000 randomized spatial and random null models.

22 We next investigated whether cortical thickness *W*-scores in iRBD were more pronounced in
23 regions with a specific functional time course and laminar organization, using respectively the Yeo
24 parcellation^{72,73} and the extended version of the von Economo and Koskinas atlas.⁷³⁻⁷⁵ The Yeo
25 parcellation attributes every region to one of seven resting-state networks (i.e., visual,
26 sensorimotor, dorsal attention, ventral attention, limbic, frontoparietal, and default-mode
27 networks), whereas the von Economo and Koskinas atlas attributes every region to one of seven
28 cortical lamination (cytoarchitectonic) classes (i.e., primary motor cortex, association cortices 1
29 and 2, primary and secondary sensory areas (dysgranular cortex), primary sensory cortex (agranular

1 cortex), limbic regions, and insular cortex). For each network and class, the cortical thickness *W*-
2 scores were averaged and tested against sets of 10,000 randomized spatial and random null models.
3 We also tested the correspondence between the patterns of cortical thickness *W*-scores in iRBD
4 and the probabilistic maps of the association between voxels and several cognitive processes. A
5 total of 123 cognitive processes from the Cognitive Atlas (<https://www.cognitiveatlas.org>)^{46,76}
6 were selected and their activation maps obtained from the meta-analytic activation maps available
7 as part of the Neurosynth database (<http://www.neurosynth.org>).⁷⁷ Neurosynth is a meta-analytic
8 tool that provides a quantitative keyword-based summary of brain activation patterns based on
9 more than 15,000 functional MRI studies. Every regional value represented the probability of each
10 of the 68 cortical regions to be activated during the functional task associated with the cognitive
11 process. Spearman's correlations were performed to test the association between cortical thickness
12 *W*-scores and the regional functional activation pattern of each cognitive process. Correlations
13 surviving the Bonferroni-corrected threshold ($P < 0.00041$) were tested against sets of 10,000
14 randomized spatial and random null models.

15 **Comparison to Alzheimer's disease (reference group)**

16 We next investigated whether the gene expression and connectivity patterns associated with
17 cortical changes in iRBD were specific to synucleinopathies or shared across the spectrum of
18 neurodegenerative diseases by performing the same analyses in a group of patients with a clinical
19 diagnosis of Alzheimer's disease. To do this, 101 patients with Alzheimer's disease and T1-
20 weighted MRI were obtained from the Alzheimer's Disease Neuroimaging Initiative database
21 (adni.loni.usc.edu).^{78,79} The Alzheimer's Disease Neuroimaging Initiative was launched in 2003 as
22 a public-private partnership, led by Principal Investigator Michael W. Weiner, MD. The primary
23 goal of the Alzheimer's Disease Neuroimaging Initiative has been to test whether the serial MRI,
24 PET, other biological markers, and clinical and neuropsychological assessment can be combined
25 to measure the progression of mild cognitive impairment and early Alzheimer's disease. The 101
26 patients with Alzheimer's disease were matched for age (66.2 ± 4.9 years) with the iRBD ($67.0 \pm$
27 6.3 years, $P = 0.24$) and control groups (66.2 ± 7.6 , $P = 0.97$) and processed similarly.¹⁵ Briefly,
28 the scans from Alzheimer's disease patients were processed using FreeSurfer 6.0, rated visually
29 based on the same previously published criteria,^{29,30} and excluded if they presented with scores >2
30 out of 4 (i.e., major reconstruction errors). This led to the exclusion of 23 patients and resulted in

1 a sample of 78 scans of patients with Alzheimer's disease (66.0 ± 4.9 years), which was also
2 matched for age to the iRBD ($P = 0.24$) and control groups ($P = 0.83$). Regional cortical thickness
3 values were extracted from these 78 surfaces, harmonized with ComBat to correct for scanner
4 variance,⁸⁰ *W*-scored to generate regional values controlled for the effects of age and sex seen in
5 controls,^{31,81} and averaged between patients to generate a vector representing the cortical thickness
6 changes associated with Alzheimer's disease. The imaging transcriptomics and comprehensive
7 spatial mapping analyses described previously were repeated to investigate whether the genetic and
8 connectivity patterns associated with cortical thickness changes in Alzheimer's disease differed
9 from those found in iRBD.

10 **Data availability**

11 The regional cortical thickness and surface area values are available at
12 <https://github.com/srahayel/SIR-RBD>.

13

14 **Results**

15 **Demographics and cortical changes in iRBD**

16 Of the 443 participants,¹⁵ 34 (7.7%) did not pass deformation-based quality control and 64 (15.6%)
17 did not pass surface-based quality control, resulting in a final sample of 138 patients and 207
18 controls from which measures of cortical morphometry were derived. All measurements were
19 converted to *W*-scores, which can be thought of as *z*-scores representing deviation from the
20 expected mean of control subjects, while correcting for age, sex, and centre.^{31,32} The groups did
21 not differ in age (iRBD: 67.0 ± 6.3 , controls: 66.2 ± 7.6 , $P = 0.28$) and sex (iRBD: 81% men,
22 controls: 77% men, $P = 0.34$, Table 1 for demographics and clinical characteristics).

23 Vertex-wise comparisons of cortical thickness between patients and controls are reported
24 elsewhere;¹⁵ they showed that iRBD patients have significant thinning in the left posterior temporal
25 and inferior parietal cortices, the left orbitofrontal and dorsolateral prefrontal cortices, and the right
26 temporal and lateral occipital cortices after controlling for age, sex, and centre and multiple
27 comparisons (Fig. 1A).¹⁵ The vertex-wise comparisons of cortical surface area, correcting
28 additionally for total intracranial volume, also revealed increased cortical surface area in iRBD

1 patients compared to controls in the left inferior temporal and entorhinal cortices (Supplementary
2 Fig. 1).¹⁵

3 **Cortical thinning associates with mitochondrial function**

4 PLS regression was performed to compare spatial patterns of gene expression versus cortical
5 thinning in iRBD. Of the five components tested, only the first explained significantly more
6 variance in thickness than random null models (60.7% versus 23.4%, $P_{random} < 0.0001$) and spatial
7 null models that preserved the spatial autocorrelation between brain regions (60.7% versus 29.9%,
8 $P_{spatial} = 0.0005$) (Fig. 1B). The regional weights of the significant component were positively
9 associated with cortical thickness W -scores in iRBD patients ($r = 0.78$, $P < 0.0001$) (Fig. 1C),
10 meaning that the genes negatively weighted on the component were more expressed in regions with
11 greater cortical thinning and that the genes positively weighted on the component were less
12 expressed in regions with greater cortical thinning (Fig. 1D).

13 We next applied GSEA to examine the translational relevance of the genes whose expression
14 overlapped with cortical thickness changes in iRBD. The genes were ranked based on bootstrap
15 ratio (Fig. 1E), and the resulting ranked gene list was intersected with several knowledge bases to
16 identify the biological processes, cellular components, and human disease gene terms enriched at
17 the top (positively weighted genes) or bottom (negatively weighted genes) of the list. In terms of
18 biological processes, the genes most strongly expressed in association with greater cortical thinning
19 (negatively weighted genes) were enriched for oxidative phosphorylation, with the most enriched
20 terms being nicotinamide adenine dinucleotide (reduced form; NADH) dehydrogenase complex
21 (complex I) assembly (normalized enrichment score: -2.44, $P_{FDR} < 0.0001$), mitochondrial
22 respiratory chain complex assembly (-2.37, $P_{FDR} < 0.0001$), and trivalent inorganic cation transport
23 (-2.32, $P_{FDR} < 0.0001$) (Fig. 2A and Table 2). Of the 15,633 genes used as input, 554 (3.5%) genes
24 were robustly associated with thickness W -scores in iRBD (i.e., bootstrap ratio weight ± 5.0), with
25 332 (60%) being negatively weighted and 222 (40%) being positively weighted (Fig. 1E). When
26 assessing the enrichment of these genes compared to the complete gene list, over-representation
27 analysis showed that the genes most strongly expressed in association with cortical thinning were
28 particularly enriched for macroautophagy (Fig. 2B).

29 In terms of cellular components, GSEA revealed that the genes more expressed in association with
30 cortical thinning were significantly enriched for components localized to the mitochondrion,

1 including the mitochondrial membrane (-2.84, $P_{FDR} < 0.0001$), respiratory chain (-2.80,
2 $P_{FDR} < 0.0001$), mitochondrial protein complex (-2.72, $P_{FDR} < 0.0001$), and NADH dehydrogenase
3 complex (-2.65, $P_{FDR} < 0.0001$) (Table 3). In terms of human disease gene terms, the genes more
4 expressed with cortical thinning in iRBD were enriched for terms related to mitochondrial diseases
5 and lactic acidosis (Table 4).

6 In contrast, the genes less strongly expressed in association with greater cortical thinning
7 (positively weighted genes) were enriched for DNA strand elongation (normalized enrichment
8 score: 2.08, $P_{FDR} = 0.015$) (Fig. 2A and Table 2) and localized to nuclear-related cellular
9 components, namely the DNA packaging complex (2.42, $P_{FDR} < 0.0001$), protein-DNA complex
10 (1.91, $P_{FDR} = 0.012$), integrator complex (1.90, $P_{FDR} = 0.009$), nuclear chromatin (1.70,
11 $P_{FDR} = 0.043$), and transcriptional repressor complex (1.69, $P_{FDR} = 0.037$) (Table 3). No human
12 disease gene terms were significantly enriched for these genes.

13 To test the robustness of our findings, we repeated the analyses using the GOrilla platform. This
14 revealed similar results (Supplementary Tables 1 and 2). When extracting gene expression from
15 different subsets of post-mortem brains, namely from the oldest brains, the older brains, and using
16 a leave-one-out procedure, we found that the negatively weighted genes predicting cortical thinning
17 in iRBD were all enriched for the same biological processes as in the main GSEA analyses (Fig.
18 2C), suggesting that the enrichment pattern associated with atrophy in iRBD is robust to variations
19 in post-mortem brain age. Finally, we explored whether the gene expression extracted from the
20 right hemisphere (2 of the 6 brains) predicted cortical thickness changes in the right hemisphere of
21 iRBD patients. We identified one component that predicted significantly more variance in cortical
22 thickness changes than null models that preserved spatial autocorrelation between brain regions
23 ($P_{spatial} = 0.028$), explaining 37.7% of the variance in cortical changes. However, in contrast to the
24 left hemisphere, the genes associated with right hemisphere cortical thinning on this component
25 were not enriched for any specific biological process.

26 Using single-cell messenger RNA sequencing data from post-mortem human brain samples,⁴⁵
27 virtual histology showed that the pattern of cortical thickness *W*-scores in iRBD patients did not
28 associate significantly with the gene expression of any of the 7 cell types investigated
29 (Supplementary Fig. 2 and Supplementary Table 3).

1 **The connectome constrains cortical changes in iRBD**

2 A diverse collection of clinical, experimental, and computational studies support that alpha-
 3 synuclein pathology behaves in a prion-like fashion,^{10,12,13,82-84} including in iRBD.¹⁵ Here, we used
 4 a structural and functional neighbourhood analysis to investigate whether the patterns of cortical
 5 thinning in iRBD were constrained by the connectome. We tested whether the thickness *W*-score
 6 of each region was dependent on the average thickness *W*-scores of its connected neighbours. We
 7 found that the greater the cortical thinning in a region in iRBD, the greater the thinning in the
 8 neighbourhood of regions sharing a structural ($r = 0.55$, $P_{spatial} = 0.013$, $P_{random} < 0.001$) or a
 9 functional connection ($r = 0.52$, $P_{spatial} = 0.011$, $P_{random} < 0.001$) (Fig. 3). In contrast, the change in
 10 local thickness was negatively related with the change in thickness observed in structurally non-
 11 connected regions ($r = -0.67$, $P_{spatial} = 0.006$, $P_{random} < 0.001$) but not significantly related with the
 12 change in thickness observed in functionally non-connected regions ($r = -0.35$, $P_{spatial} = 0.084$,
 13 $P_{random} = 0.004$) (Fig. 3). Taken together, these results support the idea that connectivity constrains
 14 thickness changes in iRBD.

15 **Cortical thinning in iRBD is associated with DAT density**

16 We next sought to determine whether the pattern of cortical changes in iRBD associated with
 17 specific neurotransmitter systems. First, we tested the relationships between the cortical thickness
 18 *W*-scores and the regional tracer density values of 18 receptors, transporters, and receptor binding
 19 sites associated with dopamine, serotonin, noradrenaline, acetylcholine, GABA, glutamate,
 20 histamine, cannabinoids, and opioids.⁴⁶ Regions that showed cortical thinning in iRBD had a lower
 21 density of DAT ($r = 0.51$, $P_{spatial} = 0.0008$, $P_{random} < 0.0001$), 5-HTT ($r = 0.51$, $P_{spatial} = 0.003$,
 22 $P_{random} < 0.0001$) and D₁ ($r = 0.39$, $P_{spatial} = 0.014$, $P_{random} = 0.0003$), and a higher density of NET
 23 ($r = -0.36$, $P_{spatial} = 0.041$, $P_{random} = 0.002$) (Fig. 4A); however, only the DAT association was
 24 significant after Bonferroni correction.

25 **Cortical thinning in iRBD maps onto the motor system**

26 We next investigated whether the patterns of cortical thickness *W*-scores in iRBD mapped onto
 27 specific resting-state networks, cytoarchitectonic classes, and functional correlates of cognition. In
 28 terms of resting-state networks, we found that cortical thinning in iRBD was more pronounced in
 29 the somatomotor (average atrophy: -0.32 , $P_{spatial} = 0.017$, $P_{random} = 0.001$) and default-mode

1 networks (-0.27 , $P_{spatial} = 0.033$, $P_{random} = 0.036$) (Fig. 4B). The correspondence with
 2 cytoarchitectonic classes revealed that cortical thinning in iRBD was more pronounced in the
 3 primary motor cortex (-0.39 , $P_{spatial} = 0.006$, $P_{random} = 0.0009$) (Fig. 4C). The correspondence
 4 between cortical thickness changes and the spatial correlates of cognitive processes also revealed
 5 a greater cortical thinning in regions more activated during tasks related to planning ($r = -0.48$,
 6 $P_{spatial} = 0.010$, $P_{random} < 0.0001$) and action ($r = -0.45$, $P_{spatial} = 0.026$, $P_{random} < 0.0001$)
 7 (Supplementary Fig. 3).

8 **Cortical thinning and surface area have distinct underlying patterns**

9 Most large-scale studies of human cortical morphometry find that cortical thickness and surface
 10 area measured by MRI are dissociable and independent.⁸⁵⁻⁸⁷ To investigate whether the gene and
 11 spatial patterns were specific to cortical thinning, we applied the same analyses to cortical surface
 12 area W -scores in iRBD. For the gene expression analyses, PLS regression identified one component
 13 that explained significantly more variance in cortical surface area W -scores than null models
 14 (random null: 42.7% versus 23.4%, $P_{random} = 0.015$; spatial null: 42.7% versus 26.3%,
 15 $P_{spatial} = 0.036$) (Supplementary Fig. 1). Positively weighted genes on the component were more
 16 expressed in association with greater surface area, whereas negatively weighed genes were less
 17 expressed in association with greater surface area (Supplementary Fig. 1). The positively weighted
 18 genes were enriched for processes involved in the inflammatory response and metal detoxification,
 19 whereas the negatively weighted genes were not significantly enriched for any biological process
 20 or cellular component gene term (Supplementary Fig. 4 and Supplementary Table 4). These
 21 enrichment patterns were similar for both gene enrichment platforms (Supplementary Tables 1 and
 22 2). When applying virtual histology, in contrast to cortical thickness, we found that greater regional
 23 cortical surface area occurred in regions with a greater expression of genes specific to astrocytes
 24 ($r = 0.61$, $P_{spatial} = 0.0011$, $P_{random} = 0.0001$), microglia ($r = 0.52$, $P_{spatial} = 0.0053$, $P_{random} = 0.001$),
 25 and oligodendrocyte precursor cells ($r = 0.53$, $P_{spatial} = 0.0049$, $P_{random} = 0.0007$) (Supplementary
 26 Fig. 2 and Supplementary Table 5).

27 For the connectivity and spatial mapping analyses, the structural and functional neighbourhood
 28 analysis showed that the regional cortical surface area W -scores in iRBD were also positively
 29 associated with the change in surface area in the regions sharing a structural ($r = 0.22$, $P_{spatial} =$
 30 0.054 , $P_{random} = 0.012$) or functional connection ($r = 0.27$, $P_{spatial} = 0.021$, $P_{random} = 0.012$)

1 (Supplementary Fig. 5), supporting that the connectome also constrains the surface area changes
 2 in iRBD but to a lesser degree. We also found that greater cortical surface area in iRBD was related
 3 to a lower density of GABA_{A/BZ}, 5-HT₆, NET, 5-HT_{1B} and M₁, and to a higher density of 5-HT_{1A}
 4 and 5-HT₄ (Supplementary Fig. 6); however, only GABA_{A/BZ} remained significant after multiple
 5 comparison correction. Finally, we found that cortical surface area was decreased in the visual
 6 resting-state network and increased in the limbic resting-state network (Supplementary Fig. 7).
 7 Cytoarchitecturally, cortical surface area was decreased in the primary and secondary sensory
 8 areas and increased in the limbic areas (Supplementary Fig. 7). Decreased cortical surface area in
 9 iRBD associated with regions more activated during tasks related to gaze and fixation
 10 (Supplementary Fig. 3). Collectively, this demonstrates that cortical thinning in iRBD is associated
 11 with gene expression and spatial mapping patterns that are different from those underlying changes
 12 in cortical surface area.

13 **Genetic and connectivity patterns are specific to synucleinopathies**

14 Next, to understand whether the patterns associated with cortical changes were specific to
 15 synucleinopathies or shared with other neurodegenerative diseases, we repeated the same analyses
 16 and investigated the genetic and connectivity underpinnings of cortical thickness changes in a
 17 sample of 78 T1-weighted MRI scans from patients with Alzheimer's disease from the Alzheimer's
 18 Disease Neuroimaging Initiative database (age: 66.0 ± 4.9 years, 38/78 (49%) men, education: 15.0
 19 ± 3.2 years, Montreal Cognitive Assessment: 23.4 ± 2.0 , 37/78 (47%) *APOE* $\epsilon 4$ heterozygous
 20 carriers, 13/78 (17%) *APOE* $\epsilon 4$ homozygous carriers).^{78,79}

21 For cortical thickness, in line with what is expected from Alzheimer's disease,^{88,89} we found that
 22 the regions that had the lowest *W*-scores (i.e., greater cortical thinning) were the entorhinal cortex
 23 (*W*-score = -0.18), medial orbitofrontal cortex (-0.13), insula (-0.12), and temporal pole (-0.10)
 24 (Supplementary Fig. 8). PLS regression revealed one component of gene expression that explained
 25 49.9% of the variance in cortical thickness changes in Alzheimer's disease ($P_{spatial} = 0.0083$, P_{random}
 26 $= 0.0028$): the genes more strongly expressed in association with cortical thinning in Alzheimer's
 27 disease were enriched for four biological processes: the protein-containing complex remodelling
 28 ($P_{FDR} = 0.0013$), with *APOE* being the gene with the largest bootstrap ratio inside this set (-7.7),
 29 the localization of proteins to the endoplasmic reticulum ($P_{FDR} = 0.0019$), RNA capping ($P_{FDR} =$
 30 0.0064), and the regulation of cyclase activity ($P_{FDR} = 0.033$) (Supplementary Table 6 and

1 Supplementary Fig. 8). These enriched terms are all different from those identified in iRBD (Fig.
 2 1C). In terms of cellular components, the gene patterns enriched in association with cortical
 3 thinning localized to the GTPase complex ($P_{FDR} = 0.024$), the glial cell projection ($P_{FDR} = 0.028$),
 4 the cytosolic part ($P_{FDR} = 0.027$), the pigment granule ($P_{FDR} = 0.038$), and the ribosome ($P_{FDR} =$
 5 0.039) (Supplementary Table 6). There were no human disease gene terms significantly associated
 6 with changes in cortical thickness in Alzheimer's disease.

7 For the spatial mapping analyses, in contrast to iRBD, greater cortical thinning was found in
 8 regions with a greater density of 5-HT_{1A} ($r = -0.69$, $P_{spatial} = 0.0003$), D2 ($r = -0.63$, $P_{spatial} <$
 9 0.0001), and μ opioid receptor ($r = -0.58$, $P_{spatial} = 0.0003$) (Supplementary Fig. 9). Cortical
 10 thinning in Alzheimer's disease appeared more prominent in the limbic resting-state network
 11 (average atrophy = -0.06 , $P_{spatial} = 0.027$) and cytoarchitectonically in the insular (average atrophy
 12 = -0.12 , $P_{spatial} = 0.015$) and limbic areas (average atrophy = -0.06 , $P_{spatial} = 0.039$) (Supplementary
 13 Fig. 9). The correspondence between cortical thickness changes and the spatial correlates of
 14 cognitive processes revealed a greater cortical thinning in regions involved in semantic memory (r
 15 = -0.49 , $P_{spatial} < 0.0001$), memory retrieval ($r = -0.46$, $P_{spatial} < 0.0001$), valence ($r = -0.46$, $P_{spatial}$
 16 = 0.0001), emotion ($r = -0.44$, $P_{spatial} = 0.0002$), thought ($r = -0.43$, $P_{spatial} = 0.0003$), and recall (r
 17 = -0.43 , $P_{spatial} = 0.0003$).

18 Taken together, these results show that the genetic and connectivity patterns underlying cortical
 19 thickness changes in iRBD differ from those associated with Alzheimer's disease, supporting that
 20 the patterns identified in iRBD are specific to synucleinopathies.

21

22 Discussion

23 Patients with iRBD demonstrate brain atrophy even prior to the development of motor and
 24 cognitive symptoms associated with synucleinopathy.^{4-6,8,9,15,90,91} Brain atrophy in iRBD is
 25 associated with motor and cognitive features, predicts conversion towards dementia, and appears
 26 to reflect the spread of abnormal alpha-synuclein isoforms in the brain.^{5,6,8,9,15,92} To better
 27 understand the pathophysiology of iRBD, we used an imaging transcriptomics approach with
 28 comprehensive spatial mapping to investigate the gene correlates and the spatial patterning of
 29 cortical thinning in iRBD. We found that cortical thinning is associated with mitochondrial function

1 and macroautophagy and that the pattern of thinning is constrained by the structural and functional
2 architecture of the connectome. We further demonstrated that the pattern of thinning maps onto
3 specific brain systems related to motor and planning functions. We also showed that these gene
4 and spatial mapping patterns were specific to cortical atrophy in iRBD in that cortical surface area
5 changes in the same patients related to different genes and brain networks. Moreover, we showed
6 that the gene and spatial mapping patterns in iRBD differed from those seen in Alzheimer's disease,
7 supporting the idea that our patterns were specific to iRBD and not shared across the
8 neurodegenerative spectrum. Altogether, this study provides insight into the processes underlying
9 the development of cortical atrophy in synucleinopathies.

10 Several pathogenic events associate with the development and progression of synucleinopathies
11 including mitochondrial dysfunction, abnormal protein degradation, and inflammation.^{93,94} In this
12 study, we found that cortical thinning in iRBD was increased in regions with a greater expression
13 of genes involved in mitochondrial functioning, particularly in the NADH dehydrogenase complex
14 (or complex I). Complex I deficiency in the substantia nigra is a hallmark of Parkinson's disease⁹⁵
15 and is found in the brain and peripheral tissues of Parkinson's disease patients.⁹⁶⁻⁹⁸ In the present
16 study, the genes that were the most robustly associated with cortical thinning in iRBD were also
17 enriched for macroautophagy, a major autophagic pathway that engulfs material to be degraded
18 into autophagosomes before fusing with lysosomes for degradation.⁹⁹ A previous study in
19 Parkinson's disease that used imaging transcriptomics to assess the gene expression correlates of
20 brain atrophy progression over 4 years found that the regions with the greatest atrophy progression
21 were enriched for genes involved in synaptic transmission and cell signalling.¹⁸ This supports the
22 sequence of events by which pathologic alpha-synuclein first interferes with mitochondrial
23 functioning, then leads to synaptic dysfunction,¹⁰⁰⁻¹⁰² and eventually manifests as cortical thinning
24 in patients, including during the prodromal period.

25 We also found that the pattern of cortical thinning in iRBD followed the constraints imposed by
26 the brain's structural and functional architecture. According to the prion-like spread hypothesis,
27 alpha-synuclein pathology propagates between cells and imposes its abnormal template onto native
28 alpha-synuclein proteins, amplifying the pathological process.⁴⁷ We recently provided evidence in
29 favour of this hypothesis using a computational spreading model of alpha-synuclein (agent-based
30 Susceptible-Infected-Removed model),¹³ showing that the distribution of alpha-synuclein
31 pathology quantified in mice injected with preformed fibrils could be recreated based on

1 connectivity and gene expression.¹⁴ Importantly, the agent-based Susceptible-Infected-Removed
2 model was also able to recreate the atrophy patterns observed in iRBD and Parkinson's disease,
3 supporting the prion-like spread model in synucleinopathies.^{13,15,16} The constraining effect of both
4 the structural and functional connectome on atrophy in iRBD is in line with this. A logical corollary
5 of this spreading hypothesis is that if alpha-synuclein pathology spreads via connections and that
6 connectivity constrains the atrophy in iRBD, then it is expected that the atrophy in iRBD maps
7 onto specific brain systems and associated intrinsic networks. This is what we observed: the pattern
8 of cortical thinning in iRBD was significantly more pronounced in the motor and default-mode
9 networks, whereas the pattern of cortical surface area changes in iRBD was more pronounced in
10 limbic and visual networks. These network findings are in line with the spatial patterning of atrophy
11 progression reported in Parkinson's disease over 2 years,¹⁸ anchoring further our atrophy pattern
12 within the prodromal spectrum of synucleinopathies.

13 In this study, a *W*-scored parcellated map of cortical changes in iRBD was used to unveil the gene
14 expression and spatial mapping underpinnings of atrophy in iRBD. This parcellated map was
15 generally convergent with the vertex-based map of cortical thickness differences between iRBD
16 patients and controls (Fig. 1A) but also showed some discrepancies. Whereas the lateral brain
17 changes were found on both maps (given the resolution difference between the two maps), the
18 medial changes, particularly in the medial frontal cortex, were not found on both maps. This may
19 be explained by the fact that the two plots differed in the method of thickness estimation and in the
20 parcellation used. The vertex-based map (Fig. 1A) was derived from an analysis performed at each
21 vertex of the cortical sheet and showed the thresholded clusters where cortical thickness was
22 significantly decreased in iRBD compared to controls after controlling for age, sex, and centre and
23 correcting for multiple comparisons. The parcellated map (Fig. 1D) represented the pattern of how
24 much the average cortical thickness in every region deviated from the expected average thickness
25 values in controls when controlling for the effects of age, sex, and centre. One interpretation for
26 the apparent discrepancy in the medial frontal cortex may be that the thickness changes occur
27 irregularly throughout this quite large region: the agglomeration of all the thickness values over
28 the region may have revealed an average pattern of thinning that was not seen when performing
29 local analysis with thresholded clustering. In other words, the smoothing extent of vertex-based
30 analyses is always by definition much smaller than the one implicit to parcellation analyses.

1 In this study, we found that the atrophy patterns in the left and right hemispheres of the brain were
2 linked to different patterns of gene expression. The atrophy in the left hemisphere was associated
3 with the expression of genes involved in energy production and waste removal, while the atrophy
4 in the right hemisphere was not significantly associated with any specific biological processes
5 (despite being significantly predicted by regional gene expression). One interpretation for this
6 observation is that the gene expression data from the right hemisphere, which came from only two
7 of the six post-mortem brains, were unreliable. Another possibility is that there is a lateralized
8 effect of gene expression in the brain whereby brain changes appear in one hemisphere in regions
9 with higher expression of genes involved in mitochondrial function and then manifest in the
10 opposite hemisphere through other prion-like mechanisms such as connectivity to the disease
11 epicentre. Also, importantly, the absence of enrichment for any specific biological processes
12 among the genes associated with atrophy in the right hemisphere does not necessarily mean that
13 these genes do not play a role in the selective vulnerability of some brain regions. It simply means
14 that the genes do not cluster around a specific function. Further research is needed to understand
15 the lateralized brain changes and their underlying causes in iRBD.

16 Our findings also revealed the presence of a dichotomy in the underlying genetic and connectomics
17 bases of cortical thinning and cortical surface area changes in iRBD. Unlike cortical thickness
18 where thinning is generally the event expected from aging and neurodegeneration,¹⁰³ surface area
19 was increased in certain areas compared to healthy individuals,¹⁵ as previously found in a
20 population-based MRI study of healthy adults showing that a higher genetic risk of Parkinson's
21 disease is associated with greater cortical surface area.¹⁰⁴ In our study, greater cortical surface area
22 was associated with a greater expression of genes involved in the inflammatory response. Similarly,
23 virtual histology revealed that increased surface area related to genes associated with astrocytes
24 and microglia. This supports the link between inflammation and synucleinopathies, particularly in
25 the prodromal stages,⁹³ where the activation of toxic microglia may lead to the production of
26 proinflammatory cytokines, which in turn produce cellular damage and cell death. In addition, we
27 found that greater surface area occurred in regions with greater expression of genes involved in
28 metal detoxification. This is in line with a study that used quantitative susceptibility mapping and
29 imaging transcriptomics and identified that the regions showing the greatest iron deposition in
30 Parkinson's disease were those with a greater expression of genes involved in metal
31 detoxification.²¹

1 That distinct gene expression and spatial mapping patterns get reflected in the thickness and surface
2 area changes in iRBD is not surprising given that thickness and surface area relate to distinct
3 genetic determinants and developmental trajectories.^{85,86} According to the radial unit hypothesis,
4 cortical thickness corresponds to the number of cells inside cortical columns, whereas cortical
5 surface area corresponds to the number of ontogenetic columns that populate perpendicularly the
6 cortex.¹⁰⁵ In addition, cortical surface area is subject to tangential expansion due to cellular
7 processes such as synaptogenesis, gliogenesis, and myelination that occur over a longer period than
8 the processes involved in cortical thickness.¹⁰⁶ Cortical thickness and surface area are differentially
9 affected in Parkinson's disease and iRBD and in healthy adults with a higher risk of Parkinson's
10 disease,^{15,104,107} but the biological explanation for this remains unclear. Based on the current study,
11 it can be hypothesized that unlike thickness, the surface area changes, which related to
12 inflammation, astrocytes, and microglia, may not necessarily relate to the pathological effects
13 occurring locally. Indeed, microglia and astrocytes are proliferating and circulating cells that can
14 take up alpha-synuclein from the extracellular space, migrate over long distances in the brain, and
15 seed pathology in remote regions.¹⁰⁸ This is supported by our neighbourhood analysis showing that
16 although the connectome exerted a constraining effect on both surface area and thickness, it
17 explained 27-30% of the variance in thickness but only 5-7% of the variance in surface area. In
18 line with that, whereas a computational spreading model of alpha-synuclein pathology based on
19 gene expression and connectivity was previously shown to recreate cortical thickness changes in
20 iRBD, it could not recreate cortical surface area changes,¹⁵ suggesting that other selective
21 vulnerability or propagation factors explain these changes. As revealed by our spatial mapping
22 analyses, one of these may be the regional density of GABA: greater surface area in iRBD mapped
23 onto regions with lower GABA_{A/BZ} receptor density. In addition to its neurotransmission role,
24 GABA modulates inflammation by regulating the proliferation of immune cells and by decreasing
25 the secretion of cytokines.^{109,110} It may therefore be that changes in cortical surface area occur in
26 regions where there is less potential for GABA to exert its immunomodulatory effects. Although
27 more studies are needed to understand the relationship between surface area and inflammation in
28 the brain of prodromal patients, it nonetheless demonstrates how an approach combining structural
29 MRI, imaging transcriptomics, and comprehensive spatial mapping can be used to generate
30 hypotheses on disease mechanisms in the prodromal phase.

1 This study has some limitations. First, the gene expression data from the Allen Human Brain Atlas
2 were extracted from post-mortem brains of people aged between 24-57 with different medical
3 histories, causes of death, and post-mortem intervals.^{34,36} Gene expression data were also
4 unavailable for the right hemisphere in 4 of the 6 post-mortem brains.³⁴ Future studies should
5 investigate more closely the gene expression predictors of atrophy from brain-wide transcriptomics
6 data extracted from post-mortem brains that were age-matched with iRBD patients and controls.
7 However, in this study, we demonstrated that the gene expression pattern predicting thinning in
8 iRBD was robust to variations in the selection of post-mortem brains. Similarly, the different brain
9 maps used for the comprehensive spatial mapping analyses were derived from participants who
10 were not age-matched to the iRBD patients and controls. Future studies should repeat the same
11 analyses using spatial maps derived from large cohorts of older participants without ongoing
12 neurodegenerative mechanism, once these become available in the literature. Second, the
13 participants who did not pass quality control after cortical surface processing were older (iRBD:
14 70.5 ± 7.3 years, controls: 68.9 ± 9.3 years) than the participants who passed quality control (iRBD:
15 67.0 ± 6.3 , controls: 66.2 ± 7.6 years, $P = 0.007$ in iRBD, $P = 0.08$ in controls). Given that the
16 quality control in both groups failed more in older people, this is unlikely to affect the findings as
17 the MRIs are used to map the distribution of atrophy of patients versus controls. In addition,
18 stringent quality control is important because they actually increase trust in findings. However, to
19 minimize the risks of sampling bias, future studies should perform more manual edits of processed
20 cortical surfaces instead of only excluding surfaces based on visual inspection. Third, the brain
21 atrophy measurements used in this work were derived from T1-weighted images. Post-mortem
22 brain examinations in Parkinson's disease have shown that alpha-synuclein pathology may present
23 first in the axonal processes before being found in cell bodies,¹¹¹ suggesting that assessment of
24 metrics from the white matter may reveal additional information about the dynamics of atrophy
25 occurring in the prodromal phase. Fourth, the interpretation of findings in this study was limited to
26 patients with a synucleinopathy in the prodromal phase. Future studies should apply a similar
27 processing and analytical framework to Parkinson's disease and dementia with Lewy bodies to
28 improve the comparability of findings between the prodromal and manifest phases of
29 synucleinopathies. Fifth, only a few iRBD patients have to date converted to a manifest
30 synucleinopathy. Once the conversion rate becomes higher, it will be possible to study the atrophy
31 patterns between conversion phenotypes.

1 In sum, the present study shows that mitochondrial and macroautophagy dysfunction underlie the
2 cortical thinning occurring in iRBD and that cortical thinning maps onto specific networks in the
3 brain.

5 **Acknowledgements**

6 Shady Rahayel reports a scholarship from the Canadian Institutes of Health Research. Jean-
7 François Gagnon holds a Canada Research Chair in Cognitive Decline in Pathological Aging. Ziv
8 Gan-Or is supported by the Fonds de recherche du Québec–Santé Chercheur-Boursier award and
9 is a William Dawson Scholar. Alain Dagher is supported by the Canadian Institutes of Health
10 Research and the Healthy Brains for Healthy Lives program of the Canada First Research
11 Excellence Fund.

12 Data used in the preparation of this article were partly obtained from the Parkinson’s Progression
13 Markers Initiative (PPMI) database (www.ppmi-info.org/access-data-specimens/download-data).
14 For up-to-date information on the study, visit www.ppmi-info.org. The PPMI – a public-private
15 partnership – is funded by the Michael J. Fox Foundation for Parkinson’s Research and funding
16 partners, including 4D Pharma, AbbVie Inc., AcureX Therapeutics, Allergan, Amathus
17 Therapeutics, Aligning Science Across Parkinson’s (ASAP), Avid Radiopharmaceuticals, Bial
18 Biotech, Biogen, BioLegend, Bristol Myers Squibb, Calico Life Sciences LLC, Celgene
19 Corporation, DaCapo Brainscience, Denali Therapeutics, The Edmond J. Safra Foundation, Eli
20 Lilly and Company, GE Healthcare, GlaxoSmithKline, Golub Capital, Handl Therapeutics, Insitro,
21 Janssen Pharmaceuticals, Lundbeck, Merck & Co., Inc., Meso Scale Diagnostics, LLC, Neurocrine
22 Biosciences, Pfizer Inc., Piramal Imaging, Prevail Therapeutics, F. Hoffman-La Roche Ltd and its
23 affiliated company Genentech Inc., Sanofi Genzyme, Servier, Takeda Pharmaceutical Company,
24 Teva Neuroscience, Inc., UCB, Vanqua Bio, Verily Life Sciences, Voyager Therapeutics, Inc., and
25 Yumanity Therapeutics, Inc.

26 For the Alzheimer’s disease data, data collection and sharing was funded by the Alzheimer’s
27 Disease Neuroimaging Initiative (ADNI) (National Institutes of Health Grant U01 AG024904) and
28 DOD ADNI (Department of Defense award number W81XWH-12-2-0012). ADNI is funded by
29 the National Institute on Aging, the National Institute of Biomedical Imaging and Bioengineering,

1 and through generous contributions from the following: AbbVie, Alzheimer’s Association;
2 Alzheimer’s Drug Discovery Foundation; Araclon Biotech; BioClinica, Inc.; Biogen; Bristol-
3 Myers Squibb Company; CereSpir, Inc.; Cogstate; Eisai Inc.; Elan Pharmaceuticals, Inc.; Eli Lilly
4 and Company; EuroImmun; F. Hoffmann-La Roche Ltd and its affiliated company Genentech,
5 Inc.; Fujirebio; GE Healthcare; IXICO Ltd.; Janssen Alzheimer Immunotherapy Research &
6 Development, LLC.; Johnson & Johnson Pharmaceutical Research & Development LLC.;
7 Lumosity; Lundbeck; Merck & Co., Inc.; Meso Scale Diagnostics, LLC.; NeuroRx Research;
8 Neurotrack Technologies; Novartis Pharmaceuticals Corporation; Pfizer Inc.; Piramal Imaging;
9 Servier; Takeda Pharmaceutical Company; and Transition Therapeutics. The Canadian Institutes
10 of Health Research is providing funds to support ADNI clinical sites in Canada. Private sector
11 contributions are facilitated by the Foundation for the National Institutes of Health (www.fnih.org).
12 The grantee organization is the Northern California Institute for Research and Education, and the
13 study is coordinated by the Alzheimer’s Therapeutic Research Institute at the University of
14 Southern California. ADNI data are disseminated by the Laboratory for Neuro Imaging at the
15 University of Southern California.

16 A portion of the data used in preparation of this article were obtained from the Alzheimer’s
17 Disease Neuroimaging Initiative (ADNI) database (adni.loni.usc.edu). As such, the investigators
18 within the ADNI contributed to the design and implementation of ADNI and/or provided data but
19 did not participate in analysis or writing of this report. A complete listing of ADNI investigators
20 can be found at: [https://adni.loni.usc.edu/wp-](https://adni.loni.usc.edu/wp-content/uploads/how_to_apply/ADNI_Acknowledgement_List.pdf)
21 [content/uploads/how_to_apply/ADNI Acknowledgement List.pdf](https://adni.loni.usc.edu/wp-content/uploads/how_to_apply/ADNI_Acknowledgement_List.pdf)

23 **Funding**

24 The work performed in Paris was funded by grants from the Programme d’investissements d’avenir
25 (ANR-10-IAIHU-06), the Paris Institute of Neurosciences – IHU (IAIHU-06), the Agence
26 Nationale de la Recherche (ANR-11-INBS-0006), Électricité de France (Fondation d’Entreprise
27 EDF), Biogen Inc., the Fondation Thérèse et René Planiol, the Fonds Saint-Michel; by unrestricted
28 support for research on Parkinson’s disease from Energipole (M. Mallart) and Société Française de
29 Médecine Esthétique (M. Legrand); and by a grant from the Institut de France to Isabelle Arnulf
30 (for the Alice Study).

1 The work performed in Montreal was supported by the Canadian Institutes of Health Research, the
2 Fonds de recherche du Québec–Santé, and the W. Garfield Weston Foundation. Jean-François
3 Gagnon reports grants from the Fonds de recherche du Québec – Santé, the Canadian Institutes of
4 Health Research, the W. Garfield Weston Foundation, the Michael J. Fox Foundation for
5 Parkinson’s Research, and the National Institutes of Health. Ronald B. Postuma reports grants and
6 personal fees from the Fonds de recherche du Québec–Santé, the Canadian Institutes of Health
7 Research, the Parkinson Society of Canada, the W. Garfield Weston Foundation, the Michael J.
8 Fox Foundation for Parkinson’s Research, the R. Howard Webster Foundation, and the National
9 Institutes of Health. Ziv Gan-Or reports funding from the Michael J. Fox Foundation, Canadian
10 Consortium for Neurodegeneration in Aging, Fonds de recherche du Québec–Santé, and ‘Healthy
11 Brains, Healthy lives’ initiative. This work was also funded by awards from the Canadian Institutes
12 of Health Research Foundation Scheme and the ‘Healthy Brain, Healthy Lives’ initiative to Alain
13 Dagher.

14 The work performed in Sydney was supported by a Dementia Team Grant from the National Health
15 and Medical Research Council (#1095127). Simon Lewis is supported by a Leadership Fellowship
16 from the National Health and Medical Research Council (#1195830). Elie Matar reports funding
17 from the National Health and Medical Research Council (#2008565). Kaylena Ehgoetz Martens
18 reports funding from Parkinson Canada, Parkinson’s Movement Disorder Foundation, University
19 of Waterloo International Research Partnership grant, and Natural Science and Engineering
20 Research Council of Canada.

21 The work performed in Aarhus was supported by funding from the Lundbeck Foundation,
22 Parkinsonforeningen (The Danish Parkinson Association), and the Jascha Foundation.

23

24 **Competing interests**

25 None of the authors report any competing interests related to the current work.

26

27 **Supplementary material**

28 Supplementary material is available at *Brain* online.

1 **Appendix 1**

2 **Contributors involved in the ICEBERG Study Group**

3 Steering committee: Marie Vidailhet, Jean-Christophe Corvol, Isabelle Arnulf, Stéphane Lehéricy.

4 Clinical data: Marie Vidailhet, Graziella Mangone, Jean-Christophe Corvol, Isabelle Arnulf, Sara
5 Sambin, Jonas Ihle, Caroline Weill, David Grabli, Florence Cormier-Dequaire, Louise Laure
6 Mariani, Bertrand Degos.

7 Neuropsychological data: Richard Levy, Fanny Pineau, Julie Socha, Eve Benchetrit, Virginie
8 Czernecki, Marie-Alexandrine Glachant.

9 Eye movement: Sophie Rivaud-Pechoux, Elodie Hainque.

10 Sleep assessment: Isabelle Arnulf, Smaranda Leu Semenescu, Pauline Dodet.

11 Genetic data: Jean-Christophe Corvol, Graziella Mangone, Samir Bekadar, Alexis Brice, Suzanne
12 Lesage.

13 Metabolomics: Fanny Mochel, Farid Ichou, Vincent Perlberg, Benoit Colsch, Arthur Tenenhaus.

14 Brain MRI data: Stéphane Lehéricy, Rahul Gaurav, Nadya Pyatigorskaya, Lydia Yahia-Cherif,
15 Romain Valabrègue, Cécile Galléa.

16 DaTscan imaging data: Marie-Odile Habert.

17 Voice recording: Dijana Petrovska, Laetitia Jeancolas.

18 Study management: Vanessa Brochard, Alizé Chalançon, Carole Dongmo-Kenfack, Christelle
19 Laganot, Valentine Maheo.

20

21

22 **References**

23 1. Postuma RB, Iranzo A, Hu M, et al. Risk and predictors of dementia and parkinsonism in
24 idiopathic REM sleep behaviour disorder: a multicentre study. *Brain*. Mar 1 2019;142(3):744-759.
25 doi:10.1093/brain/awz030

- 1 2. Hogl B, Stefani A, Videnovic A. Idiopathic REM sleep behaviour disorder and
2 neurodegeneration - an update. *Nat Rev Neurol.* Jan 2018;14(1):40-55.
3 doi:10.1038/nrneurol.2017.157
- 4 3. Bourgooin PA, Rahayel S, Gaubert M, et al. Neuroimaging of Rapid Eye Movement Sleep
5 Behavior Disorder. *Int Rev Neurobiol.* 2019;144:185-210. doi:10.1016/bs.irm.2018.10.006
- 6 4. Campabadal A, Segura B, Junque C, Iranzo A. Structural and functional magnetic
7 resonance imaging in isolated REM sleep behavior disorder: A systematic review of studies using
8 neuroimaging software. *Sleep Med Rev.* Apr 22 2021;59:101495. doi:10.1016/j.smrv.2021.101495
- 9 5. Rahayel S, Postuma RB, Montplaisir J, et al. Abnormal Gray Matter Shape, Thickness, and
10 Volume in the Motor Cortico-Subcortical Loop in Idiopathic Rapid Eye Movement Sleep Behavior
11 Disorder: Association with Clinical and Motor Features. *Cereb Cortex.* Feb 1 2018;28(2):658-671.
12 doi:10.1093/cercor/bhx137
- 13 6. Rahayel S, Postuma RB, Montplaisir J, et al. Cortical and subcortical gray matter bases of
14 cognitive deficits in REM sleep behavior disorder. *Neurology.* May 15 2018;90(20):e1759-e1770.
15 doi:10.1212/WNL.0000000000005523
- 16 7. Campabadal A, Segura B, Junque C, et al. Comparing the accuracy and neuroanatomical
17 correlates of the UPSIT-40 and the Sniffin' Sticks test in REM sleep behavior disorder.
18 *Parkinsonism Relat Disord.* Aug 2019;65:197-202. doi:10.1016/j.parkreldis.2019.06.013
- 19 8. Pereira JB, Weintraub D, Chahine L, Aarsland D, Hansson O, Westman E. Cortical thinning
20 in patients with REM sleep behavior disorder is associated with clinical progression. *NPJ*
21 *Parkinsons Dis.* 2019;5:7. doi:10.1038/s41531-019-0079-3
- 22 9. Rahayel S, Postuma RB, Montplaisir J, et al. A Prodromal Brain-Clinical Pattern of
23 Cognition in Synucleinopathies. *Ann Neurol.* Feb 2021;89(2):341-357. doi:10.1002/ana.25962
- 24 10. Kordower JH, Chu Y, Hauser RA, Freeman TB, Olanow CW. Lewy body-like pathology
25 in long-term embryonic nigral transplants in Parkinson's disease. *Nat Med.* May 2008;14(5):504-
26 6. doi:10.1038/nm1747
- 27 11. Gonzalez-Rodriguez P, Zampese E, Surmeier DJ. Selective neuronal vulnerability in
28 Parkinson's disease. *Prog Brain Res.* 2020;252:61-89. doi:10.1016/bs.pbr.2020.02.005

- 1 12. Luk KC, Kehm V, Carroll J, et al. Pathological alpha-synuclein transmission initiates
2 Parkinson-like neurodegeneration in nontransgenic mice. *Science*. Nov 16 2012;338(6109):949-
3 53. doi:10.1126/science.1227157
- 4 13. Zheng YQ, Zhang Y, Yau Y, et al. Local vulnerability and global connectivity jointly shape
5 neurodegenerative disease propagation. *PLoS Biol*. Nov 2019;17(11):e3000495.
6 doi:10.1371/journal.pbio.3000495
- 7 14. Rahayel S, Misic B, Zheng YQ, et al. Differentially targeted seeding reveals unique
8 pathological alpha-synuclein propagation patterns. *Brain*. Jun 3 2022;145(5):1743-1756.
9 doi:10.1093/brain/awab440
- 10 15. Rahayel S, Tremblay C, Vo A, et al. Brain atrophy in prodromal synucleinopathy is shaped
11 by structural connectivity and gene expression. *Brain*. May 20 2022;doi:10.1093/brain/awac187
- 12 16. Abdelgawad A, Rahayel S, Zheng Y-Q, et al. Predicting longitudinal brain atrophy in
13 Parkinson's disease using a Susceptible-Infected-Removed agent-based model. *medRxiv*.
14 2022:2022.05.01.22274521. doi:10.1101/2022.05.01.22274521
- 15 17. Arnatkeviciute A, Markello RD, Fulcher BD, Misic B, Fornito A. Towards Best Practices
16 for Imaging Transcriptomics of the Human Brain. *Biological Psychiatry*. 2022/11/05/
17 2022;doi:https://doi.org/10.1016/j.biopsych.2022.10.016
- 18 18. Tremblay C, Rahayel S, Vo A, et al. Brain atrophy progression in Parkinson's disease is
19 shaped by connectivity and local vulnerability. *medRxiv*. 2021:2021.06.08.21258321.
20 doi:10.1101/2021.06.08.21258321
- 21 19. Freeze B, Pandya S, Zeighami Y, Raj A. Regional transcriptional architecture of
22 Parkinson's disease pathogenesis and network spread. *Brain*. Oct 1 2019;142(10):3072-3085.
23 doi:10.1093/brain/awz223
- 24 20. Maia PD, Pandya S, Freeze B, et al. Origins of atrophy in Parkinson linked to early onset
25 and local transcription patterns. *Brain Commun*. 2020;2(2):fcaa065.
26 doi:10.1093/braincomms/fcaa065
- 27 21. Thomas GEC, Zarkali A, Ryten M, et al. Regional brain iron and gene expression provide
28 insights into neurodegeneration in Parkinson's disease. *Brain*. Jul 28 2021;144(6):1787-1798.
29 doi:10.1093/brain/awab084

- 1 22. Brown JA, Deng J, Neuhaus J, et al. Patient-Tailored, Connectivity-Based Forecasts of
2 Spreading Brain Atrophy. *Neuron*. Dec 4 2019;104(5):856-868 e5.
3 doi:10.1016/j.neuron.2019.08.037
- 4 23. Tetreault AM, Phan T, Orlando D, et al. Network localization of clinical, cognitive, and
5 neuropsychiatric symptoms in Alzheimer's disease. *Brain*. Apr 1 2020;143(4):1249-1260.
6 doi:10.1093/brain/awaa058
- 7 24. Marek K, Chowdhury S, Siderowf A, et al. The Parkinson's progression markers initiative
8 (PPMI) - establishing a PD biomarker cohort. *Ann Clin Transl Neurol*. Dec 2018;5(12):1460-1477.
9 doi:10.1002/acn3.644
- 10 25. American Academy of Sleep Medicine. The International Classification of Sleep Disorders
11 — Third Edition (ICSD-3). vol 3rd ed. American Academy of Sleep Medicine; 2014.
- 12 26. Postuma RB, Berg D, Stern M, et al. MDS clinical diagnostic criteria for Parkinson's
13 disease. *Mov Disord*. Oct 2015;30(12):1591-601. doi:10.1002/mds.26424
- 14 27. McKeith IG, Boeve BF, Dickson DW, et al. Diagnosis and management of dementia with
15 Lewy bodies: Fourth consensus report of the DLB Consortium. *Neurology*. Jul 4 2017;89(1):88-
16 100. doi:10.1212/WNL.0000000000004058
- 17 28. Gilman S, Wenning GK, Low PA, et al. Second consensus statement on the diagnosis of
18 multiple system atrophy. *Neurology*. Aug 26 2008;71(9):670-6.
19 doi:10.1212/01.wnl.0000324625.00404.15
- 20 29. Klapwijk ET, van de Kamp F, van der Meulen M, Peters S, Wierenga LM. Qoala-T: A
21 supervised-learning tool for quality control of FreeSurfer segmented MRI data. *Neuroimage*. Apr
22 1 2019;189:116-129. doi:10.1016/j.neuroimage.2019.01.014
- 23 30. Monereo-Sanchez J, de Jong JJA, Drenthen GS, et al. Quality control strategies for brain
24 MRI segmentation and parcellation: Practical approaches and recommendations - insights from the
25 Maastricht study. *Neuroimage*. Aug 15 2021;237:118174. doi:10.1016/j.neuroimage.2021.118174
- 26 31. Tremblay C, Abbasi N, Zeighami Y, et al. Sex effects on brain structure in de novo
27 Parkinson's disease: a multimodal neuroimaging study. *Brain*. Oct 1 2020;143(10):3052-3066.
28 doi:10.1093/brain/awaa234

- 1 32. La Joie R, Perrotin A, Barre L, et al. Region-specific hierarchy between atrophy,
2 hypometabolism, and beta-amyloid (A β) load in Alzheimer's disease dementia. *J Neurosci*. Nov
3 14 2012;32(46):16265-73. doi:10.1523/JNEUROSCI.2170-12.2012
- 4 33. Barnes J, Ridgway GR, Bartlett J, et al. Head size, age and gender adjustment in MRI
5 studies: a necessary nuisance? *Neuroimage*. Dec 2010;53(4):1244-55.
6 doi:10.1016/j.neuroimage.2010.06.025
- 7 34. Hawrylycz MJ, Lein ES, Guillozet-Bongaarts AL, et al. An anatomically comprehensive
8 atlas of the adult human brain transcriptome. *Nature*. Sep 20 2012;489(7416):391-399.
9 doi:10.1038/nature11405
- 10 35. Markello RD, Arnatkeviciute A, Poline JB, Fulcher BD, Fornito A, Misic B. Standardizing
11 workflows in imaging transcriptomics with the abagen toolbox. *Elife*. Nov 16
12 2021;10doi:10.7554/eLife.72129
- 13 36. Arnatkeviciute A, Fulcher BD, Fornito A. A practical guide to linking brain-wide gene
14 expression and neuroimaging data. *Neuroimage*. Apr 1 2019;189:353-367.
15 doi:10.1016/j.neuroimage.2019.01.011
- 16 37. Quackenbush J. Microarray data normalization and transformation. *Nat Genet*. Dec
17 2002;32 Suppl:496-501. doi:10.1038/ng1032
- 18 38. Hawrylycz M, Miller JA, Menon V, et al. Canonical genetic signatures of the adult human
19 brain. *Nat Neurosci*. Dec 2015;18(12):1832-44. doi:10.1038/nn.4171
- 20 39. Fulcher BD, Little MA, Jones NS. Highly comparative time-series analysis: the empirical
21 structure of time series and their methods. *J R Soc Interface*. Jun 6 2013;10(83):20130048.
22 doi:10.1098/rsif.2013.0048
- 23 40. Vasa F, Misic B. Null models in network neuroscience. *Nat Rev Neurosci*. Aug
24 2022;23(8):493-504. doi:10.1038/s41583-022-00601-9
- 25 41. Efron B, Tibshirani R. Bootstrap methods for standard errors, confidence intervals, and
26 other measures of statistical accuracy. *Stat Sci*. 1986;1:54-77.

- 1 42. Liao Y, Wang J, Jaehnig EJ, Shi Z, Zhang B. WebGestalt 2019: gene set analysis toolkit
2 with revamped UIs and APIs. *Nucleic Acids Res.* Jul 2 2019;47(W1):W199-W205.
3 doi:10.1093/nar/gkz401
- 4 43. Subramanian A, Tamayo P, Mootha VK, et al. Gene set enrichment analysis: a knowledge-
5 based approach for interpreting genome-wide expression profiles. *Proc Natl Acad Sci U S A.* Oct
6 25 2005;102(43):15545-50. doi:10.1073/pnas.0506580102
- 7 44. Eden E, Navon R, Steinfeld I, Lipson D, Yakhini Z. GOrilla: a tool for discovery and
8 visualization of enriched GO terms in ranked gene lists. *BMC Bioinformatics.* Feb 3 2009;10:48.
9 doi:10.1186/1471-2105-10-48
- 10 45. Seidlitz J, Nadig A, Liu S, et al. Transcriptomic and cellular decoding of regional brain
11 vulnerability to neurogenetic disorders. *Nat Commun.* Jul 3 2020;11(1):3358. doi:10.1038/s41467-
12 020-17051-5
- 13 46. Hansen JY, Shafiei G, Markello RD, et al. Mapping neurotransmitter systems to the
14 structural and functional organization of the human neocortex. *Nat Neurosci.* Oct 27
15 2022;doi:10.1038/s41593-022-01186-3
- 16 47. Peng C, Trojanowski JQ, Lee VM. Protein transmission in neurodegenerative disease. *Nat*
17 *Rev Neurol.* Apr 2020;16(4):199-212. doi:10.1038/s41582-020-0333-7
- 18 48. Cammoun L, Gigandet X, Meskaldji D, et al. Mapping the human connectome at multiple
19 scales with diffusion spectrum MRI. *J Neurosci Methods.* Jan 30 2012;203(2):386-97.
20 doi:10.1016/j.jneumeth.2011.09.031
- 21 49. Shafiei G, Markello RD, Makowski C, et al. Spatial Patterning of Tissue Volume Loss in
22 Schizophrenia Reflects Brain Network Architecture. *Biol Psychiatry.* Apr 15 2020;87(8):727-735.
23 doi:10.1016/j.biopsych.2019.09.031
- 24 50. Hansen JY, Shafiei G, Vogel JW, et al. Local molecular and global connectomic
25 contributions to cross-disorder cortical abnormalities. *Nat Commun.* Aug 10 2022;13(1):4682.
26 doi:10.1038/s41467-022-32420-y
- 27 51. Shafiei G, Bazinet V, Dadar M, et al. Network structure and transcriptomic vulnerability
28 shape atrophy in frontotemporal dementia. *Brain.* Feb 21 2022;doi:10.1093/brain/awac069

- 1 52. Betzel RF, Griffa A, Hagmann P, Misisic B. Distance-dependent consensus thresholds for
2 generating group-representative structural brain networks. *Netw Neurosci.* 2019;3(2):475-496.
3 doi:10.1162/netn_a_00075
- 4 53. Kaller S, Rullmann M, Patt M, et al. Test-retest measurements of dopamine D1-type
5 receptors using simultaneous PET/MRI imaging. *Eur J Nucl Med Mol Imaging.* Jun
6 2017;44(6):1025-1032. doi:10.1007/s00259-017-3645-0
- 7 54. Sandiego CM, Gallezot JD, Lim K, et al. Reference region modeling approaches for
8 amphetamine challenge studies with [11C]FLB 457 and PET. *J Cereb Blood Flow Metab.* Mar 31
9 2015;35(4):623-9. doi:10.1038/jcbfm.2014.237
- 10 55. Smith CT, Crawford JL, Dang LC, et al. Partial-volume correction increases estimated
11 dopamine D2-like receptor binding potential and reduces adult age differences. *J Cereb Blood Flow*
12 *Metab.* May 2019;39(5):822-833. doi:10.1177/0271678X17737693
- 13 56. Dukart J, Holiga S, Chatham C, et al. Cerebral blood flow predicts differential
14 neurotransmitter activity. *Sci Rep.* Mar 6 2018;8(1):4074. doi:10.1038/s41598-018-22444-0
- 15 57. Savli M, Bauer A, Mitterhauser M, et al. Normative database of the serotonergic system in
16 healthy subjects using multi-tracer PET. *Neuroimage.* Oct 15 2012;63(1):447-59.
17 doi:10.1016/j.neuroimage.2012.07.001
- 18 58. Gallezot JD, Nabulsi N, Neumeister A, et al. Kinetic modeling of the serotonin 5-HT(1B)
19 receptor radioligand [(11)C]P943 in humans. *J Cereb Blood Flow Metab.* Jan 2010;30(1):196-210.
20 doi:10.1038/jcbfm.2009.195
- 21 59. Beliveau V, Ganz M, Feng L, et al. A High-Resolution In Vivo Atlas of the Human Brain's
22 Serotonin System. *J Neurosci.* Jan 4 2017;37(1):120-128. doi:10.1523/JNEUROSCI.2830-16.2016
- 23 60. Radhakrishnan R, Nabulsi N, Gaiser E, et al. Age-Related Change in 5-HT6 Receptor
24 Availability in Healthy Male Volunteers Measured with (11)C-GSK215083 PET. *J Nucl Med.* Sep
25 2018;59(9):1445-1450. doi:10.2967/jnumed.117.206516
- 26 61. Ding YS, Singhal T, Planeta-Wilson B, et al. PET imaging of the effects of age and cocaine
27 on the norepinephrine transporter in the human brain using (S,S)-[(11)C]O-methylreboxetine and
28 HRRT. *Synapse.* Jan 2010;64(1):30-8. doi:10.1002/syn.20696

- 1 62. Hillmer AT, Esterlis I, Gallezot JD, et al. Imaging of cerebral alpha4beta2* nicotinic
2 acetylcholine receptors with (-)-[(18)F]Flubatine PET: Implementation of bolus plus constant
3 infusion and sensitivity to acetylcholine in human brain. *Neuroimage*. Nov 1 2016;141:71-80.
4 doi:10.1016/j.neuroimage.2016.07.026
- 5 63. Naganawa M, Nabulsi N, Henry S, et al. First-in-Human Assessment of (11)C-
6 LSN3172176, an M1 Muscarinic Acetylcholine Receptor PET Radiotracer. *J Nucl Med*. Apr
7 2021;62(4):553-560. doi:10.2967/jnumed.120.246967
- 8 64. Aghourian M, Legault-Denis C, Soucy JP, et al. Quantification of brain cholinergic
9 denervation in Alzheimer's disease using PET imaging with [(18)F]-FEOBV. *Mol Psychiatry*. Nov
10 2017;22(11):1531-1538. doi:10.1038/mp.2017.183
- 11 65. Bedard MA, Aghourian M, Legault-Denis C, et al. Brain cholinergic alterations in
12 idiopathic REM sleep behaviour disorder: a PET imaging study with (18)F-FEOBV. *Sleep Med*.
13 Jun 2019;58:35-41. doi:10.1016/j.sleep.2018.12.020
- 14 66. Norgaard M, Beliveau V, Ganz M, et al. A high-resolution in vivo atlas of the human brain's
15 benzodiazepine binding site of GABAA receptors. *Neuroimage*. May 15 2021;232:117878.
16 doi:10.1016/j.neuroimage.2021.117878
- 17 67. DuBois JM, Rousset OG, Rowley J, et al. Characterization of age/sex and the regional
18 distribution of mGluR5 availability in the healthy human brain measured by high-resolution
19 [(11)C]ABP688 PET. *Eur J Nucl Med Mol Imaging*. Jan 2016;43(1):152-162. doi:10.1007/s00259-
20 015-3167-6
- 21 68. Smart K, Cox SML, Scala SG, et al. Sex differences in [(11)C]ABP688 binding: a positron
22 emission tomography study of mGlu5 receptors. *Eur J Nucl Med Mol Imaging*. May
23 2019;46(5):1179-1183. doi:10.1007/s00259-018-4252-4
- 24 69. Gallezot JD, Planeta B, Nabulsi N, et al. Determination of receptor occupancy in the
25 presence of mass dose: [(11)C]GSK189254 PET imaging of histamine H3 receptor occupancy by
26 PF-03654746. *J Cereb Blood Flow Metab*. Mar 2017;37(3):1095-1107.
27 doi:10.1177/0271678X16650697
- 28 70. Normandin MD, Zheng MQ, Lin KS, et al. Imaging the cannabinoid CB1 receptor in
29 humans with [11C]OMAR: assessment of kinetic analysis methods, test-retest reproducibility, and

- 1 gender differences. *J Cereb Blood Flow Metab.* Aug 2015;35(8):1313-22.
2 doi:10.1038/jcbfm.2015.46
- 3 71. Kantonen T, Karjalainen T, Isojarvi J, et al. Interindividual variability and lateralization of
4 mu-opioid receptors in the human brain. *Neuroimage.* Aug 15 2020;217:116922.
5 doi:10.1016/j.neuroimage.2020.116922
- 6 72. Yeo BT, Krienen FM, Sepulcre J, et al. The organization of the human cerebral cortex
7 estimated by intrinsic functional connectivity. *J Neurophysiol.* Sep 2011;106(3):1125-65.
8 doi:10.1152/jn.00338.2011
- 9 73. Vazquez-Rodriguez B, Suarez LE, Markello RD, et al. Gradients of structure-function
10 tethering across neocortex. *Proc Natl Acad Sci U S A.* Oct 15 2019;116(42):21219-21227.
11 doi:10.1073/pnas.1903403116
- 12 74. Scholtens LH, de Reus MA, de Lange SC, Schmidt R, van den Heuvel MP. An MRI Von
13 Economo - Koskinas atlas. *Neuroimage.* Apr 15 2018;170:249-256.
14 doi:10.1016/j.neuroimage.2016.12.069
- 15 75. Vertes PE, Rittman T, Whitaker KJ, et al. Gene transcription profiles associated with inter-
16 modular hubs and connection distance in human functional magnetic resonance imaging networks.
17 *Philos Trans R Soc Lond B Biol Sci.* Oct 5 2016;371(1705)doi:10.1098/rstb.2015.0362
- 18 76. Poldrack RA, Kittur A, Kalar D, et al. The cognitive atlas: toward a knowledge foundation
19 for cognitive neuroscience. *Front Neuroinform.* 2011;5:17. doi:10.3389/fninf.2011.00017
- 20 77. Yarkoni T, Poldrack RA, Nichols TE, Van Essen DC, Wager TD. Large-scale automated
21 synthesis of human functional neuroimaging data. *Nat Methods.* Jun 26 2011;8(8):665-70.
22 doi:10.1038/nmeth.1635
- 23 78. Aisen PS, Petersen RC, Donohue MC, et al. Clinical Core of the Alzheimer's Disease
24 Neuroimaging Initiative: progress and plans. *Alzheimers Dement.* May 2010;6(3):239-46.
25 doi:10.1016/j.jalz.2010.03.006
- 26 79. Veitch DP, Weiner MW, Aisen PS, et al. Understanding disease progression and improving
27 Alzheimer's disease clinical trials: Recent highlights from the Alzheimer's Disease Neuroimaging
28 Initiative. *Alzheimers Dement.* Jan 2019;15(1):106-152. doi:10.1016/j.jalz.2018.08.005

- 1 80. Fortin JP, Cullen N, Sheline YI, et al. Harmonization of cortical thickness measurements
2 across scanners and sites. *Neuroimage*. Feb 15 2018;167:104-120.
3 doi:10.1016/j.neuroimage.2017.11.024
- 4 81. Radua J, Vieta E, Shinohara R, et al. Increased power by harmonizing structural MRI site
5 differences with the ComBat batch adjustment method in ENIGMA. *Neuroimage*. Sep
6 2020;218:116956. doi:10.1016/j.neuroimage.2020.116956
- 7 82. Rey NL, George S, Steiner JA, et al. Spread of aggregates after olfactory bulb injection of
8 alpha-synuclein fibrils is associated with early neuronal loss and is reduced long term. *Acta*
9 *Neuropathol*. Jan 2018;135(1):65-83. doi:10.1007/s00401-017-1792-9
- 10 83. Recasens A, Dehay B, Bove J, et al. Lewy body extracts from Parkinson disease brains
11 trigger alpha-synuclein pathology and neurodegeneration in mice and monkeys. *Ann Neurol*. Mar
12 2014;75(3):351-62. doi:10.1002/ana.24066
- 13 84. Li JY, Englund E, Holton JL, et al. Lewy bodies in grafted neurons in subjects with
14 Parkinson's disease suggest host-to-graft disease propagation. *Nat Med*. May 2008;14(5):501-3.
15 doi:10.1038/nm1746
- 16 85. Hogstrom LJ, Westlye LT, Walhovd KB, Fjell AM. The structure of the cerebral cortex
17 across adult life: age-related patterns of surface area, thickness, and gyrification. *Cereb Cortex*.
18 Nov 2013;23(11):2521-30. doi:10.1093/cercor/bhs231
- 19 86. Grasby KL, Jahanshad N, Painter JN, et al. The genetic architecture of the human cerebral
20 cortex. *Science*. Mar 20 2020;367(6484)doi:10.1126/science.aay6690
- 21 87. Panizzon MS, Fennema-Notestine C, Eyler LT, et al. Distinct genetic influences on cortical
22 surface area and cortical thickness. *Cereb Cortex*. Nov 2009;19(11):2728-35.
23 doi:10.1093/cercor/bhp026
- 24 88. Braak H, Braak E. Neuropathological staging of Alzheimer-related changes. *Acta*
25 *Neuropathol*. 1991;82(4):239-59. doi:10.1007/BF00308809
- 26 89. Holbrook AJ, Tustison NJ, Marquez F, et al. Anterolateral entorhinal cortex thickness as a
27 new biomarker for early detection of Alzheimer's disease. *Alzheimers Dement (Amst)*.
28 2020;12(1):e12068. doi:10.1002/dad2.12068

- 1 90. Rahayel S, Montplaisir J, Monchi O, et al. Patterns of cortical thinning in idiopathic rapid
2 eye movement sleep behavior disorder. *Mov Disord.* Apr 15 2015;30(5):680-7.
3 doi:10.1002/mds.25820
- 4 91. Holtbernd F, Romanzetti S, Oertel WH, et al. Convergent patterns of structural brain
5 changes in rapid eye movement sleep behavior disorder and Parkinson's disease on behalf of the
6 German rapid eye movement sleep behavior disorder study group. *Sleep.* Mar 12
7 2021;44(3)doi:10.1093/sleep/zsaa199
- 8 92. Campabadal A, Segura B, Junque C, et al. Cortical Gray Matter and Hippocampal Atrophy
9 in Idiopathic Rapid Eye Movement Sleep Behavior Disorder. *Front Neurol.* 2019;10:312.
10 doi:10.3389/fneur.2019.00312
- 11 93. Tansey MG, Wallings RL, Houser MC, Herrick MK, Keating CE, Joers V. Inflammation
12 and immune dysfunction in Parkinson disease. *Nat Rev Immunol.* Mar 4 2022;doi:10.1038/s41577-
13 022-00684-6
- 14 94. Haelterman NA, Yoon WH, Sandoval H, Jaiswal M, Shulman JM, Bellen HJ. A mitocentric
15 view of Parkinson's disease. *Annu Rev Neurosci.* 2014;37:137-59. doi:10.1146/annurev-neuro-
16 071013-014317
- 17 95. Gonzalez-Rodriguez P, Zampese E, Stout KA, et al. Disruption of mitochondrial complex
18 I induces progressive parkinsonism. *Nature.* Nov 2021;599(7886):650-656. doi:10.1038/s41586-
19 021-04059-0
- 20 96. Subrahmanian N, LaVoie MJ. Is there a special relationship between complex I activity and
21 nigral neuronal loss in Parkinson's disease? A critical reappraisal. *Brain Res.* Sep 15
22 2021;1767:147434. doi:10.1016/j.brainres.2021.147434
- 23 97. Parker WD, Jr., Parks JK, Swerdlow RH. Complex I deficiency in Parkinson's disease
24 frontal cortex. *Brain Res.* Jan 16 2008;1189:215-8. doi:10.1016/j.brainres.2007.10.061
- 25 98. Keeney PM, Xie J, Capaldi RA, Bennett JP, Jr. Parkinson's disease brain mitochondrial
26 complex I has oxidatively damaged subunits and is functionally impaired and misassembled. *J*
27 *Neurosci.* May 10 2006;26(19):5256-64. doi:10.1523/JNEUROSCI.0984-06.2006
- 28 99. Griffey CJ, Yamamoto A. Macroautophagy in CNS health and disease. *Nat Rev Neurosci.*
29 May 3 2022;doi:10.1038/s41583-022-00588-3

- 1 100. Merino-Galan L, Jimenez-Urbieta H, Zamarbide M, et al. Striatal synaptic bioenergetic and
2 autophagic decline in premotor experimental parkinsonism. *Brain*. Mar 4
3 2022;doi:10.1093/brain/awac087
- 4 101. Grassi D, Howard S, Zhou M, et al. Identification of a highly neurotoxic alpha-synuclein
5 species inducing mitochondrial damage and mitophagy in Parkinson's disease. *Proc Natl Acad Sci*
6 *U S A*. Mar 13 2018;115(11):E2634-E2643. doi:10.1073/pnas.1713849115
- 7 102. Volpicelli-Daley LA, Luk KC, Patel TP, et al. Exogenous alpha-synuclein fibrils induce
8 Lewy body pathology leading to synaptic dysfunction and neuron death. *Neuron*. Oct 6
9 2011;72(1):57-71. doi:10.1016/j.neuron.2011.08.033
- 10 103. Fjell AM, Westlye LT, Grydeland H, et al. Accelerating cortical thinning: unique to
11 dementia or universal in aging? *Cereb Cortex*. Apr 2014;24(4):919-34. doi:10.1093/cercor/bhs379
- 12 104. Abbasi N, Tremblay C, Rajimehr R, et al. Neuroanatomical correlates of polygenic risk for
13 Parkinson's Disease. *medRxiv*. 2022:2022.01.17.22269262. doi:10.1101/2022.01.17.22269262
- 14 105. Rakic P. Radial unit hypothesis of neocortical expansion. *Novartis Found Symp*.
15 2000;228:30-42; discussion 42-52. doi:10.1002/0470846631.ch3
- 16 106. Cafiero R, Brauer J, Anwander A, Friederici AD. The Concurrence of Cortical Surface Area
17 Expansion and White Matter Myelination in Human Brain Development. *Cereb Cortex*. Feb 1
18 2019;29(2):827-837. doi:10.1093/cercor/bhy277
- 19 107. Laansma MA, Bright JK, Al-Bachari S, et al. International Multicenter Analysis of Brain
20 Structure Across Clinical Stages of Parkinson's Disease. *Mov Disord*. Nov 2021;36(11):2583-
21 2594. doi:10.1002/mds.28706
- 22 108. Steiner JA, Quansah E, Brundin P. The concept of alpha-synuclein as a prion-like protein:
23 ten years after. *Cell Tissue Res*. Jul 2018;373(1):161-173. doi:10.1007/s00441-018-2814-1
- 24 109. Jin Z, Mendu SK, Birnir B. GABA is an effective immunomodulatory molecule. *Amino*
25 *Acids*. Jul 2013;45(1):87-94. doi:10.1007/s00726-011-1193-7
- 26 110. Crowley T, Cryan JF, Downer EJ, O'Leary OF. Inhibiting neuroinflammation: The role and
27 therapeutic potential of GABA in neuro-immune interactions. *Brain Behav Immun*. May
28 2016;54:260-277. doi:10.1016/j.bbi.2016.02.001

1 111. Braak H, Sandmann-Keil D, Gai W, Braak E. Extensive axonal Lewy neurites in
2 Parkinson's disease: a novel pathological feature revealed by alpha-synuclein
3 immunocytochemistry. *Neurosci Lett.* Apr 9 1999;265(1):67-9. doi:10.1016/s0304-
4 3940(99)00208-6

5 **Figure legends**

6 **Figure 1 Patterns of gene expression underlying cortical thinning in iRBD.** (A) Vertex-wise
7 patterns showing the significant changes in cortical thickness in iRBD patients compared to
8 controls. (B) Violin plots showing the percentage of variance in cortical thickness *W*-scores
9 explained by gene expression; the dot represents the empirical variance, and the asterisk indicates
10 the components that were significant against random and spatial null models. (C) Scatterplot of the
11 association between thickness *W*-scores and the regional weights of the first component. (D) Brain
12 renderings of the thickness *W*-scores and the regional weights of the first component. (E) Density
13 plots of each gene's bootstrapped weight on the first component; gene set enrichment analysis was
14 performed on all genes, whereas over-representation analysis was performed on genes with
15 bootstrap ratios ± 5.0 . C = component; iRBD = isolated rapid eye movement sleep behaviour
16 disorder; RM = random null models; SM = spatial null models.

17
18 **Figure 2 Enrichment analyses of the genes associated with cortical thinning in iRBD.** (A) The
19 top 10 biological process terms from the GO Consortium knowledge base that are enriched in the
20 positively and negatively weighted gene sets predicting cortical thinning in iRBD. Terms are
21 ranked based on the normalized enrichment score; darker coloured bars present significantly
22 enriched terms after FDR correction. (B) Volcano plot of the over-representation analysis showing
23 the biological process terms enriched in the genes most strongly associated with cortical thinning
24 in iRBD (bootstrap ratio < -5.0). The colour bar represents the number of overlapping edges for
25 each gene category and the size of the dot represents the size of the gene category. (C) Additional
26 gene enrichment analyses performed on different subsets of post-mortem brains (different gene
27 expression matrices) showed that the enriched patterns in association with cortical thinning in
28 iRBD were stable and different from Alzheimer's disease. The upper grid represents the different
29 post-mortem brains selected for each analysis, with blue and red circles representing respectively
30 brains from male and female donors. The lower grid represents the top 10 biological process terms

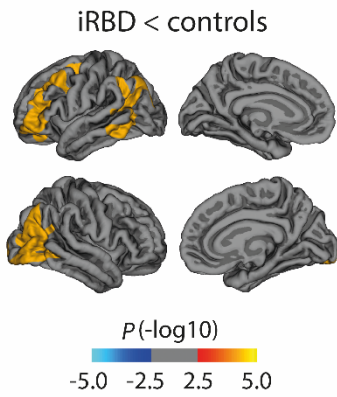
1 obtained in each analysis, with numbers representing the respective ranking of the term based on
2 the normalized enrichment score. FDR = false discovery rate; GO = Gene Ontology; iRBD =
3 isolated rapid eye movement sleep behaviour disorder; NADH = nicotinamide adenine dinucleotide
4 (reduced form).

5
6 **Figure 3 The connectome constrains cortical thinning in iRBD.** Brain renderings showing the
7 associations between the deviation in cortical thickness W -scores in iRBD and (A) structural and
8 (B) functional connectivity. The edge thickness on the brain plots represents the interregional
9 connection strength, whereas the node size and colour represent the local deviation in the W -score
10 in iRBD compared to controls (i.e., the larger and redder, the greater the change in thickness). The
11 scatterplots show the associations, for connected regions and non-connected regions, between the
12 deviations in W -scores and the average W -scores observed in structural or functional neighbours.
13 The violin plots show the empirical correlation against sets of 10,000 correlations generated from
14 spatial and random null models. The asterisk indicates associations that were significant against
15 null models. iRBD = isolated rapid eye movement sleep behaviour disorder.

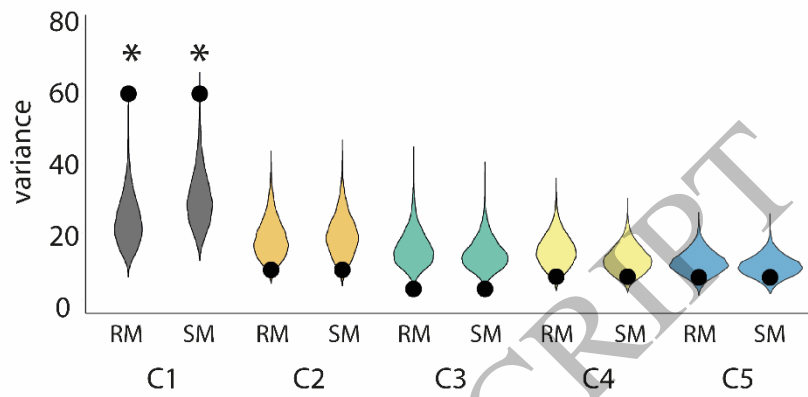
16
17 **Figure 4 Cortical thinning in iRBD map onto specific regional tracer density, resting-state**
18 **networks, and cytoarchitectonic classes.** (A) Brain renderings and scatterplots showing the tracer
19 density maps of the receptors, transporters, and binding sites associated with cortical thickness W -
20 scores in iRBD. The violin plots show the empirical correlations tested against distributions of
21 correlations from sets of spatial and random null models. The asterisk indicates the significant
22 associations after Bonferroni correction. Radar charts showing the correlation between cortical
23 thickness W -scores in iRBD and (B) resting-state networks and (C) cytoarchitectonic classes. The
24 regular line represents the empirical correlations, and the dashed line represents the average
25 correlation observed in sets of 10,000 spatial null models. The asterisk indicates the networks and
26 classes where the observed spatial correlation was significantly different from the null correlation.
27 5HTT = serotonin transporter; DAT = dopamine active transporter; iRBD = isolated rapid eye
28 movement sleep behaviour disorder; NET = noradrenaline transporter.

29
30

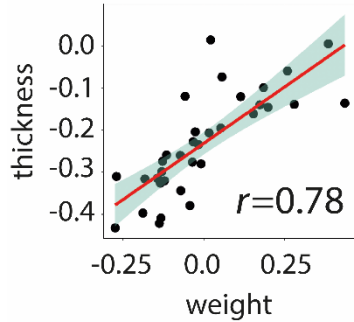
A cortical thickness



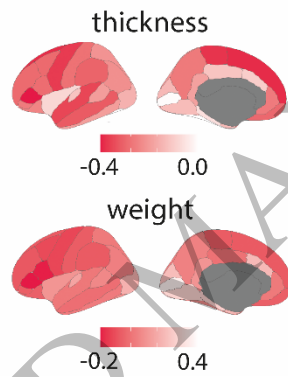
B partial least squares regression



C first component



D brain plots



E bootstrap histogram

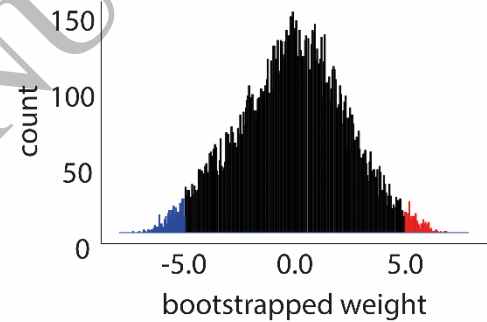
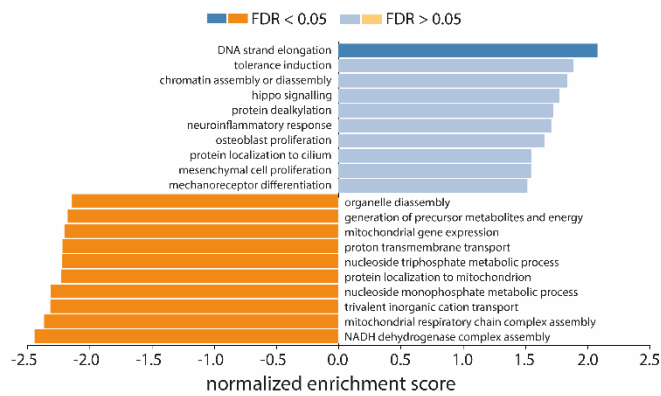


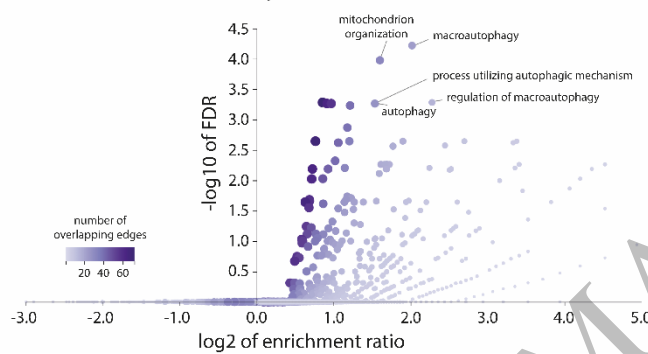
Figure 1
166x125 mm (x DPI)

1
2
3
4

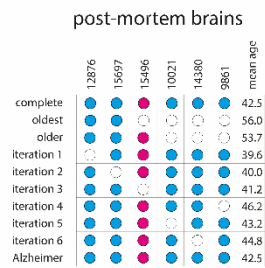
A gene set enrichment analysis



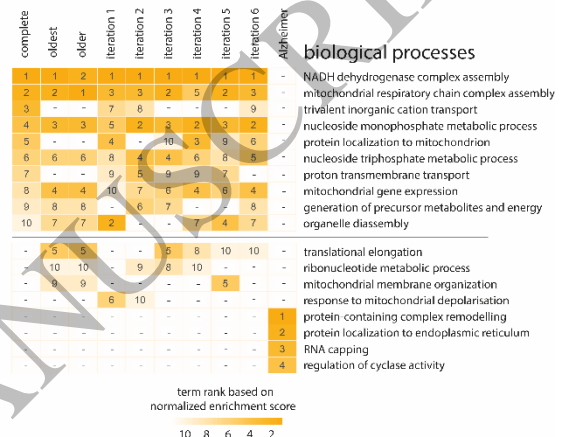
B over-enrichment analysis



C gene expression subsets



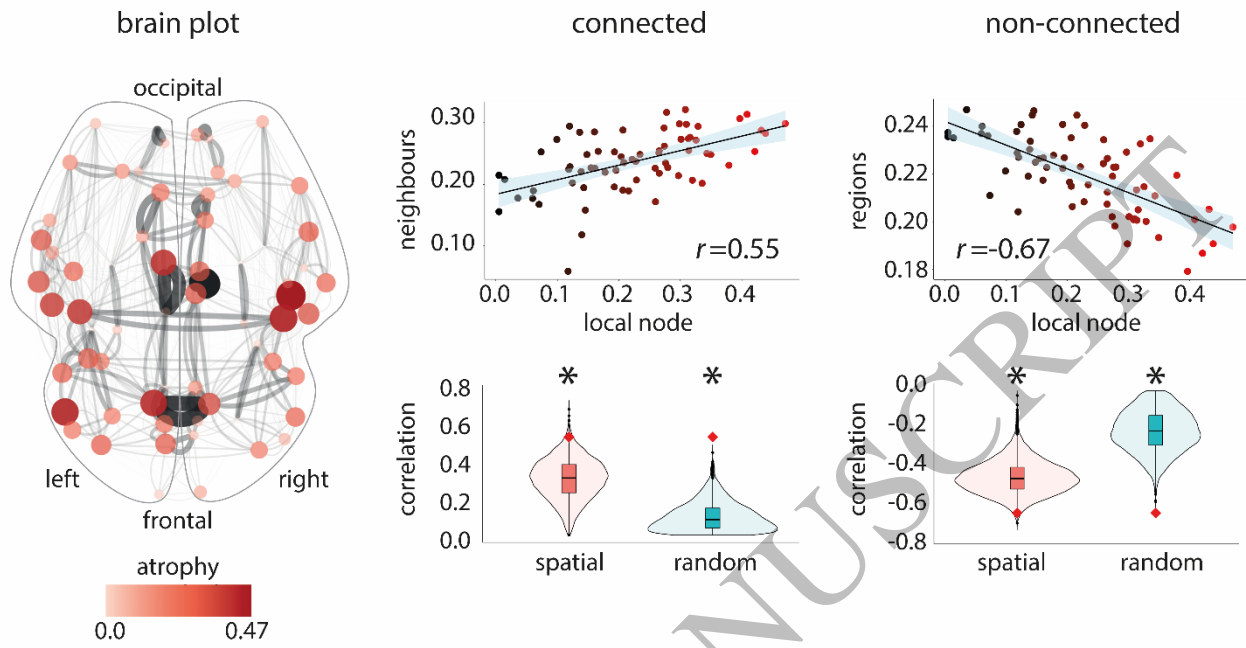
enrichment pattern (top 10 terms)



- 1
- 2
- 3
- 4

Figure 2
166x110 mm (x DPI)

A structural connectome



B functional connectome

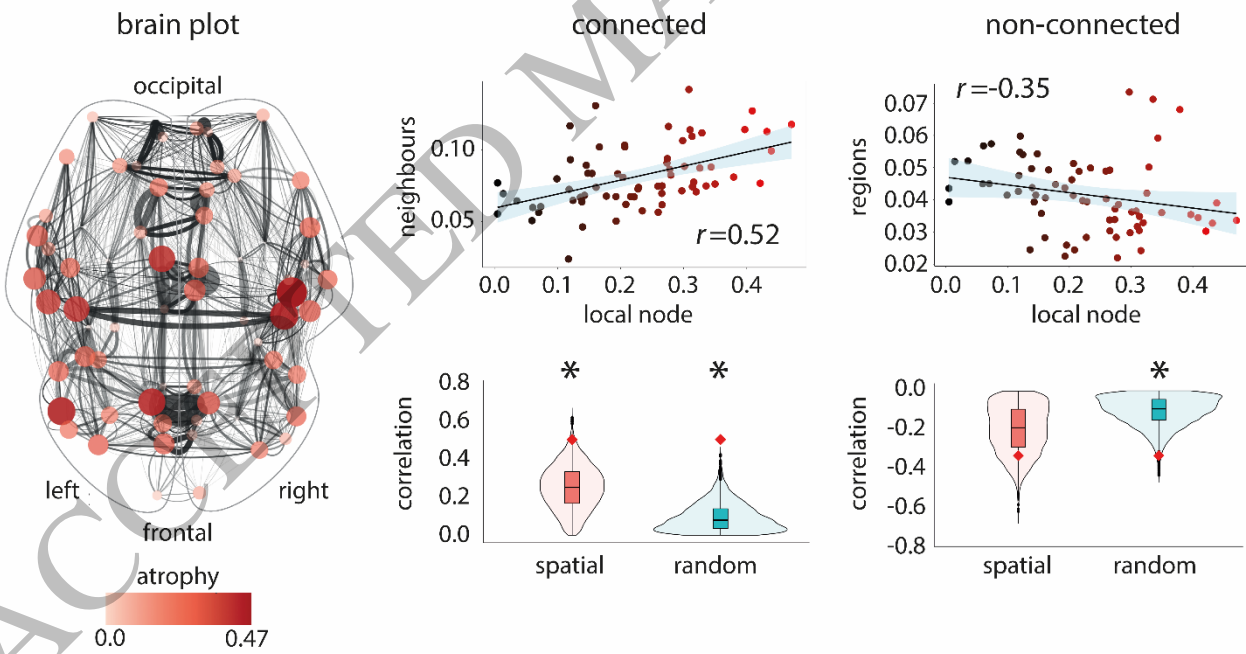
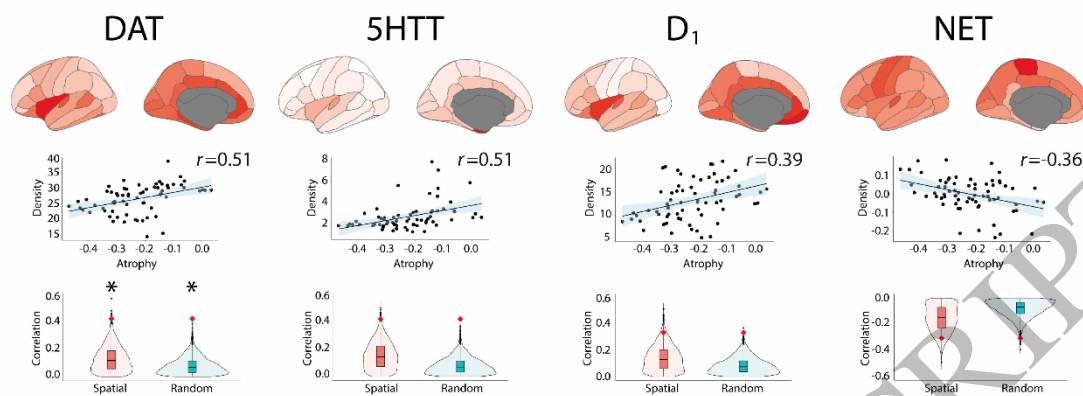


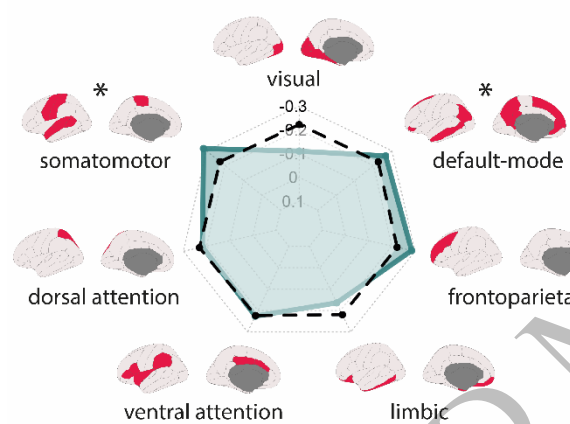
Figure 3
166x189 mm (x DPI)

1
2
3
4

A neurotransmitter systems



B resting-state networks



C cytoarchitectonic classes

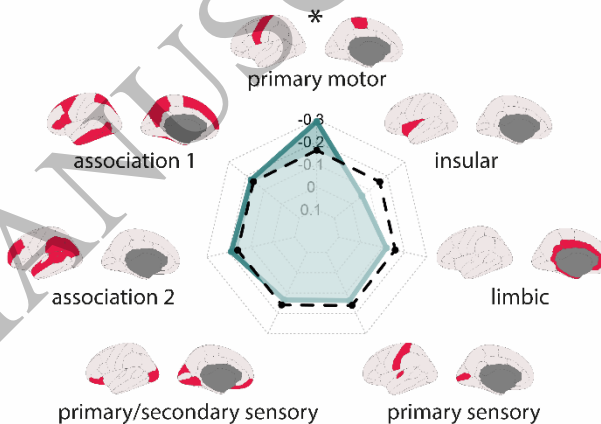


Figure 4
166x124 mm (x DPI)

1
2
3
4

1 **Table I Demographics and clinical variables of the cohorts after quality control**

Cohort	iRBD patients	Controls	P value
Total cohort, n	138	207	
Age (SD)	67.0 (6.3)	66.2 (7.6)	0.28
Sex, n (% men)	112 (81)	159 (77)	0.34
MoCA	26.4 (2.8)	27.8 (1.7)	<0.001
MDS-UPDRS-III	7.1 (6.6)	2.0 (3.5)	<0.001
Paris cohort, n	41	37	
Age (SD)	66.6 (5.6)	64.9 (7.3)	0.27
Sex, n (% men)	36 (88)	30 (81)	0.41
MoCA	26.8 (3.0)	27.2 (2.3)	0.45
MDS-UPDRS-III	8.7 (6.9)	3.6 (4.8)	<0.001
Montreal cohort, n	48	35	
Age (SD)	65.8 (6.4)	65.0 (7.1)	0.57
Sex, n (% men)	37 (77)	21 (60)	0.09
MoCA	25.9 (2.7)	28.2 (1.4)	<0.001
UPDRS-III ^a	4.3 (3.6)	-	<0.001
Sydney cohort, n	14	22	
Age (SD)	67.0 (8.0)	70.0 (5.3)	0.23
Sex, n (% men)	12 (86)	14 (64)	0.26
MoCA	27.1 (2.3)	-	-
MDS-UPDRS-III	11.0 (5.7)	-	-
Aarhus cohort, n	16	19	
Age (SD)	68.2 (6.9)	67.8 (5.9)	0.87
Sex, n (% men)	13 (81)	14 (74)	0.70
MoCA	27.1 (2.1)	27.1 (2.1)	0.92
MDS-UPDRS-III	1.1 (1.5)	-	-
PPMI cohort, n	19	94	
Age (SD)	70.1 (5.3)	66.0 (8.4)	0.010
Sex, n (% men)	14 (74)	80 (85)	0.23
MoCA	25.8 (3.4)	28.2 (1.2)	0.009
MDS-UPDRS-III	5.5 (6.0)	1.3 (2.5)	0.008

2 The subjects presented here are those after quality control. Data are presented as mean (SD). P values in bold represent significant differences.
3 iRBD = isolated rapid eye movement sleep behaviour disorder; MDS = Movement Disorders Society; MoCA = Montreal Cognitive Assessment;
4 PPMI = Parkinson's Progression Markers Initiative; SD = standard deviation; UPDRS-III = Unified Parkinson's Disease Rating Scale, motor
5 examination.

6 ^aFahn & Elton UPDRS-III version (1987).
7

1 **Table 2 Biological processes enriched in the genes predicting cortical thinning in iRBD.**

GO identifier	GO term	Gene set size	Number of leading edge IDs	Enrichment score	Normalized enrichment score	FDR P value
Negatively weighted (more expressed) genes						
GO:0010257	NADH dehydrogenase complex assembly	58	44	-0.622	-2.442	<0.0001
GO:0033108	mitochondrial respiratory chain complex assembly	88	57	-0.551	-2.365	<0.0001
GO:0072512	trivalent inorganic cation transport	32	14	-0.668	-2.315	<0.0001
GO:0009123	nucleoside monophosphate metabolic process	275	126	-0.467	-2.313	<0.0001
GO:0070585	protein localization to mitochondrion	132	53	-0.492	-2.227	0.00019
GO:0009141	nucleoside triphosphate metabolic process	262	120	-0.450	-2.220	0.00016
GO:1902600	proton transmembrane transport	121	53	-0.498	-2.218	0.00014
GO:0140053	mitochondrial gene expression	158	69	-0.476	-2.203	0.00012
GO:0006091	generation of precursor metabolites and energy	405	173	-0.420	-2.175	0.00011
GO:1903008	organelle disassembly	93	50	-0.509	-2.142	0.00028
Positively weighted (less expressed) genes						
GO:0022616	DNA strand elongation	21	11	0.638	2.081	0.015
GO:0002507	tolerance induction	13	7	0.664	1.889	0.093
GO:0006333	chromatin assembly or disassembly	119	37	0.392	1.838	0.102
GO:0035329	hippo signalling	32	19	0.486	1.777	0.140
GO:0008214	protein dealkylation	31	14	0.473	1.727	0.182
GO:0150076	neuroinflammatory response	32	12	0.472	1.709	0.176
GO:0033687	osteoblast proliferation	21	12	0.507	1.656	0.240
GO:0061512	protein localization to cilium	39	12	0.407	1.550	0.265
GO:0010463	mesenchymal cell proliferation	34	13	0.430	1.548	0.252
GO:0042490	mechanoreceptor differentiation	44	15	0.380	1.517	0.267

2 The top 10 biological process terms enriched in the genes predicting cortical thinning in iRBD are reported ranked based on the normalized
3 enrichment score. Bold values represent the terms significantly enriched after applying FDR correction. FDR = false discovery rate; GO = Gene
4 Ontology; NADH = nicotinamide adenine dinucleotide (reduced form); iRBD = isolated rapid eye movement sleep behaviour disorder.

5

6

1 **Table 3 Cellular components enriched in the genes predicting cortical thinning in iRBD**

GO identifier	GO term	Gene set size	Number of leading edge IDs	Enrichment score	Normalized enrichment score	FDR P value
Negatively weighted (more expressed) genes						
GO:0044455	mitochondrial membrane part	206	128	-0.589	-2.843	<0.0001
GO:0070469	respiratory chain	86	61	-0.656	-2.799	<0.0001
GO:0098798	mitochondrial protein complex	248	135	-0.554	-2.724	<0.0001
GO:0030964	NADH dehydrogenase complex	45	35	-0.699	-2.645	<0.0001
GO:0005743	mitochondrial inner membrane	414	200	-0.501	-2.596	<0.0001
GO:0016469	proton-transporting two-sector ATPase complex	40	22	-0.689	-2.497	<0.0001
GO:0070069	cytochrome complex	27	17	-0.682	-2.258	<0.0001
GO:1905368	peptidase complex	85	37	-0.526	-2.230	<0.0001
GO:0005759	mitochondrial matrix	432	183	-0.428	-2.230	<0.0001
GO:0043209	myelin sheath	152	75	-0.473	-2.179	<0.0001
Positively weighted (less expressed) genes						
GO:0044815	DNA packaging complex	52	34	0.598	2.416	<0.0001
GO:0032993	protein-DNA complex	129	46	0.400	1.911	0.012
GO:0032039	integrator complex	17	6	0.611	1.900	0.009
GO:0000790	nuclear chromatin	297	111	0.320	1.704	0.043
GO:0017053	transcriptional repressor complex	78	27	0.384	1.693	0.037
GO:0005790	smooth endoplasmic reticulum	31	16	0.445	1.602	0.068
GO:0044450	microtubule organizing center part	155	38	0.325	1.588	0.064
GO:0016605	PML body	91	20	0.335	1.514	0.079
GO:0005697	telomerase holoenzyme complex	19	9	0.477	1.502	0.079
GO:0045178	basal part of cell	41	19	0.395	1.501	0.073

2 The top 10 cellular component terms enriched in the genes predicting cortical thickness changes in iRBD are reported ranked based on the
3 normalized enrichment score. Bold values represent the terms significantly enriched after applying FDR correction. FDR = false discovery rate;
4 GO = Gene Ontology; iRBD = isolated rapid eye movement sleep behaviour disorder; NADH = nicotinamide adenine dinucleotide (reduced
5 form); PML = promyelocytic leukaemia.

6
7

1 **Table 4 Human disease gene terms enriched in the genes predicting cortical thinning in iRBD**

Term	Description	Gene set size	Number of leading edge IDs	Enrichment score	Normalized enrichment score	FDR P value
Negatively weighted (more expressed) genes						
DisGeNET						
C0001125	Acidosis, Lactic	87	48	-0.606	-2.586	<0.0001
C0347959	Lactic acidemia	85	47	-0.602	-2.550	<0.0001
C1167918	CSF lactate increased	33	22	-0.690	-2.410	<0.0001
C0006114	Cerebral edema	23	15	-0.702	-2.230	<0.001
C0023264	Leigh disease	33	21	-0.629	-2.216	<0.001
C0424551	Impaired exercise tolerance	42	22	-0.599	-2.211	<0.001
C1836440	Increased serum lactate	52	27	-0.571	-2.178	0.001
C4021546	Abnormal mitochondria in muscle tissue	17	12	-0.751	-2.177	0.001
C1145670	Respiratory failure	73	40	-0.528	-2.149	0.002
C1855020	Acute necrotizing encephalopathy	14	11	-0.771	-2.126	0.003
OMIM						
252010	Mitochondrial complex I deficiency	20	15	-0.640	-2.019	<0.001
PharmGKB						
PA447172	Mitochondrial diseases	349	161	-0.464	-2.352	<0.0001
PA166048819	Acidosis, Respiratory	78	49	-0.552	-2.300	<0.0001
PA443242	Acidosis	117	66	-0.514	-2.281	<0.0001
PA445837	Thiamine deficiency	54	25	-0.570	-2.201	0.001
PA165108683	Pyruvate dehydrogenase complex deficiency	26	12	-0.657	-2.197	<0.001
PA443243	Acidosis, Lactic	64	24	-0.544	-2.196	<0.001
PA447190	Cytochrome-c oxidase deficiency	55	30	-0.555	-2.168	0.002
PA446467	Mitochondrial encephalomyopathies	48	24	-0.572	-2.146	0.002
PA165857066	Anemia, Hemolytic, Congenital Nonspherocytic	10	7	-0.820	-2.082	0.006
PA165108373	Biotinidase deficiency	44	22	-0.558	-2.077	0.006

2 The human disease terms enriched in the genes predicting cortical thinning in iRBD using the DisGeNET, OMIM, and PharmGKB knowledge bases.
 3 Terms are reported ranked based on the normalized enrichment score. Only terms enriched after applying FDR correction are shown. FDR =
 4 false discovery rate; iRBD = isolated rapid eye movement sleep behaviour disorder; OMIM = Online Mendelian Inheritance in Man.

5
6
7